Assessing the effects of warming and carbonate chemistry parameters on marine microbes in the Gulf of Mexico through basin-scale DNA metabarcoding

Sean R. Anderson[1,2*], Katherine Silliman[4], Leticia Barbero[3,4], Fabian A. Gomez[7,8], Beth A. Stauffer[5], Astrid Schnetzer[6], Christopher R. Kelble[4,†], and Luke R. Thompson[4,7*]

[1]Department of Biological Sciences, University of New Hampshire, Durham, NH, USA

[2]Marine Chemistry and Geochemistry Department, Woods Hole Oceanographic Institution, Falmouth, MA, USA

[3]Cooperative Institute for Marine and Atmospheric Studies, University of Miami, Miami, FL, USA

[4]National Oceanic and Atmospheric Administration, Atlantic Oceanographic and Meteorological Laboratory, Ocean Chemistry and Ecosystems Division, Miami, FL, USA

[5]Department of Biology, University of Louisiana at Lafayette, Lafayette, LA, USA

[6]Marine, Earth, and Atmospheric Sciences, North Carolina State University, Raleigh, NC, USA

[7]Northern Gulf Institute, Mississippi State University, Starkville, MS, USA

[8]Physical Oceanography Division, Atlantic Oceanographic and Meteorological Laboratory, Miami, FL, USA

[†]National Oceanic and Atmospheric Administration, National Marine Fisheries Service, Office of Science and Technology

*Corresponding authors: Sean R. Anderson and Luke R. Thompson

Emails: sean.anderson1@unh.edu and luke.thompson@noaa.gov

Keywords: Metabarcoding; Ocean Acidification; Warming; Microbes; Protists; Bacteria; Archaea; Gulf of Mexico; Generalized linear models; Indicator analysis

Abstract

Ocean acidification and warming threaten marine life, yet the impact of these processes on microbes remains unclear. Here, we performed basin-scale DNA metabarcoding of prokaryotes (16S V4–V5) and protists (18S V9) in the Gulf of Mexico and applied generalized linear models to reveal group-specific environmental correlates of functionally diverse microbes. Models supported prior physiological trends for some groups, like positive temperature effects on SAR11 and SAR86, and a positive effect of pH on *Prochlorococcus* that implied a negative response to decreasing pH. New insights were revealed for protists, like Syndiniales and Sagenista (e.g., positive pH effects), which offset positive relationships with temperature and reinforced the importance of considering multiple stressors simultaneously. Indicator analysis revealed phytoplankton, like *Ostreococcus* sp. and *Emiliania huxleyi*, that were associated with more acidic waters and may reflect candidate indicators of ocean change. Our findings highlight the need for sustained microbial sampling in marine systems, with implications for carbon export, nutrient cycling, and ecosystem health.

Introduction

Our ability to predict how marine ecosystems and resources will respond to future ocean conditions will require accurate monitoring of marine biodiversity over space, time, and across natural environmental gradients (*1*). The oceans are changing rapidly, heavily impacted by rising concentrations of human-derived atmospheric carbon dioxide (CO_2) that is absorbed at the ocean's surface (*2*). Atmospheric CO_2 has increased by nearly 50% (~420 ppm at present) over the last century, leading to increased levels of dissolved inorganic carbon (DIC) in the ocean, in turn lowering seawater pH (*3*). This process of ocean acidification (OA) reduces saturation states for carbonate minerals, placing stress on organisms that require these minerals for cellular growth and other functions (*4*, *5*). The effects of OA are amplified by ocean warming, particularly at low latitudes, with surface temperatures expected to increase by 1–10 °C over the next century (*6*). Changes in seawater chemistry and physics can have immense impacts, both direct and indirect, on marine life (*3*). Thus, it is imperative to understand better how diverse marine organisms respond to present-day chemical and physical conditions to inform future potential shifts in community composition.

Over the past decade, research on species sensitivity to OA has expanded greatly, particularly for multicellular organisms that rely on carbonate chemistry for their structure and function (*3*, *5*). Much less research has been conducted on marine microbes (i.e., protists, Bacteria, and Archaea), despite the central role of microbes in food webs and their strong influence on biogeochemical cycles and carbon export (*7*, *8*). Microbes also respond quickly to shifts in their surrounding environment, making them potentially important indicators of changing ocean conditions (*9*, *10*). In general, global ecosystem models predict a decline in photosynthetic biomass and a shift in composition from larger plankton (e.g., diatoms) to picophytoplankton

(0.2–2 μm), primarily driven by warming and enhanced stratification (*11–14*). Field and laboratory experiments have measured direct and negative impacts of OA on plankton, notably among calcifying haptophytes (e.g., coccolithophores), where increased partial pressure of CO_2 (pCO_2) and/or decreasing pH has led to reduced growth and calcification rates (*15–17*). However, evidence suggests that some phytoplankton species, even coccolithophores, may be resilient to rising pCO_2 and warming (*13*, *18*, *19*). In addition, heterotrophic bacteria may be more resilient to OA compared to phytoplankton, impacted more directly by warming and changes to phytoplankton-derived organic matter (*20*, *21*). Employing DNA metabarcoding to characterize the complex effects of OA parameters and temperature on a wide range of microbes (*22*, *23*) will help guide lab-based experiments, identify indicator taxa, and inform model predictions.

The Gulf of Mexico (GOM) is an ideal location to study the effects of multiple stressors on marine microbes, as microbial communities in the GOM are affected by several major hydrographic features that result in strong physicochemical gradients (*24*). The GOM is a semi-enclosed subtropical basin, influenced by the Loop Current (and associated anticyclonic eddies) and freshwater inflow from riverine systems (Mississippi-Atchafalaya) in the north (*25*, *26*). Most of the GOM is oligotrophic (and nutrient-limited), with phytoplankton biomass dominated by picophytoplankton (*27*). Despite overall low biomass, microbial food webs in the GOM support high biodiversity of mesozooplankton and micronekton (*28*), as well as several economically important fisheries (*29*). At times, nutrient runoff from terrestrial sources promotes eutrophication, resulting in coastal hypoxic zones that are more acidic (*30*, *31*). Coastal eutrophication combined with physical upwelling of new inorganic nutrients onto the shelf can also enhance formation of harmful algal blooms (HABs), particularly along the western coast of Florida (*32*, *33*) and in other coastal regions in the southern Gulf (*34*). HABs pose a threat to marine ecosystems in the GOM and can negatively impact local economies (*35*). While OA has resulted in observable changes in ocean chemistry in the GOM (*24*), research on the impacts of OA and warming on marine microbes has not been well explored. Most microbial genomics studies have been localized to specific regions or depths (*36–39*) or focused on responses of microbes to natural disturbances, like oil spills, in the northern Gulf (*40*, *41*). This lack of spatial biological sampling has made it difficult to characterize environmental drivers of diverse microbes in the GOM (*24*), including OA parameters (e.g., pH, DIC, and pCO_2), and impedes our ability to understand how microbial communities may shift in the future.

Here, we performed the first basin-scale DNA metabarcoding survey of protists, Bacteria, and Archaea in the GOM as part of the fourth Gulf of Mexico Ecosystems and Carbon Cycle (GOMECC-4) cruise that sailed from late summer to early fall of 2021. Overall, we collected 481 discrete DNA samples from 51 (out of 141) stations, encompassing 16 inshore–offshore transects and up to three depths per site that corresponded to the surface, deep chlorophyll maximum (DCM), and near bottom (Fig. 1A). Amplicon metabarcoding was performed to reveal population dynamics of protists (18S SSU rRNA gene, V9 region) and prokaryotes (16S SSU

rRNA gene, V4–V5 region). We constructed generalized linear models (GLMs) for major microbial groups in the photic zone to gain insight into group-specific environmental correlates, including carbonate system parameters. These GLMs were applied to all GOMECC-4 sites, including those where DNA samples were not collected, to expand spatial distributions of microbial groups in the GOM. Finally, we performed indicator analysis based on profiles of DIC and total alkalinity (TA) in the photic zone to identify microbes that were potential indicators of more or less acidic waters (based on TA:DIC ratios). This study provides an important baseline for microbial OA research in the GOM that will guide future DNA sampling efforts in this region and contribute to our growing knowledge on the potential responses of marine microbes to climate change.

Results and Discussion

Microbial population dynamics in the GOM

We obtained a total of 8,312 sequences on average per sample (range: 3,322–16,483) from 18S metabarcoding, resulting in 13,632 protist amplicon sequence variants (ASVs) identified throughout all GOM samples. In comparison, we obtained an average of 12,963 sequences per sample (range: 5,056–28,620) for 16S metabarcoding which were assigned to 41,876 total prokaryotic ASVs. Though significant to community composition ($P < 0.01$), factors like transect, location on the shelf (< 200 m) vs. open ocean (> 200 m), and categorical depth had low explanatory power on their own (PERMANOVA $R = 0.03–0.2$). As depth is a well-known driver of global marine microbial communities (*42–46*), we performed hierarchical clustering of microbial composition to better control for the impact of depth on subsequent spatial analyses. This revealed separation of DNA samples into three clusters (Clusters 1–3), similar for both marker gene regions, that reflected depth of samples in the water column on the continental shelf and/or in open ocean GOM regions (Fig. 1B; fig. S1). For instance, Cluster 1 mainly consisted of samples collected on the shelf at all depths and offshore at the surface layer, with all samples located in the photic zone (2–99 m). Cluster 2 samples were mainly from the DCM (2–124 m) in more stratified open ocean regions of the GOM, while Cluster 3 samples largely represented meso- to bathypelagic waters (135–3,326 m) in the open ocean that were confined to the aphotic zone (Fig. 2A–B; Fig. 3A–B). Though Clusters 1–2 were both in the photic zone (upper ~150 m), and had some overlap (Fig. 2B), they were separated into distinct clusters based on their composition that reflected total depth in the water column and shifts in physicochemical variables (fig. S2). In our case, clustering of DNA samples allowed us to better explore microbes, and their relationships with environmental variables, within distinct spatial habitats they occupy in the GOM.

Microbial communities in the GOM were more species-rich and diverse in the DCM and aphotic zone (Fig. 2C; Fig. 3C), consistent with vertical profiles from other oceanic regions (*43*, *46*, *47*). Higher richness and diversity with depth may be the result of microbes utilizing a broad

spectrum of sinking organic matter, exerting alternative metabolic strategies (redox reactions), and/or forming diverse trophic relationships with other organisms to exploit such habitats (*48*). Alpha diversity was stable along sampling transects in the photic zone for 16S (fig. S3) and 18S samples (fig. S4), with higher variability in the DCM and aphotic zone. For example, microbial diversity in the aphotic zone steadily decreased from coastal Florida (27°N line) to regions near the Mississippi River outflow, increasing thereafter from Brownsville to Cancun (fig. S3).

Shifts in taxonomy between clusters were in line with depth-related microbial dynamics seen previously in the GOM (*37*, *38*, *49*) and on a global scale (*42*, *43*, *48*). Among prokaryotes, the photic zone and DCM were dominated by common heterotrophic bacteria, such as SAR11, SAR86, and Flavobacteriales (Fig. 2D; fig. S5). Autotrophic cyanobacteria within the order Synechococcales also had high relative abundance in the photic zone (Fig. 2D; fig. S5), particularly *Prochlorococcus* and *Synechococcus* (fig. S6), both genera known to dominate primary production in the GOM (*27*). Prokaryotic communities shifted dramatically in the aphotic zone, with higher relative abundance of metabolically diverse taxa that are endemic to deeper waters (*48–50*), including nitrous oxide-reducing Marinimicrobia (SAR406), ammonia-oxidizing Nitrosopumilales, and sulfur-oxidizing Thiomicrospirales (Fig. 2D; fig. S5). These microbes use redox reactions to acquire energy in less oxygenated waters (*48*), such as those found in the mesopelagic zone (~200–800 m) in the GOM (fig. S2), and likely contributed to increased richness of prokaryotic communities observed with depth (Fig. 2C). Certain 16S groups varied at more resolved taxonomic levels between clusters. For example, *Prochlorococcus* became more relatively abundant in the DCM, while SAR11 clade II increased in the aphotic zone relative to other SAR11 clades (fig. S7). Similar patterns have been observed elsewhere for *Prochlorococcus* (*51*) and SAR11 (*48*, *52*), and reflect potential environmental niche partitioning through the water column. High abundance of SAR11 clade II in the mesopelagic has recently been observed in the Pacific Ocean (*48*), which may indicate particle association among SAR11 that may be more common than previously thought.

Protist biodiversity was dominated by Dinophyceae, Syndiniales, Prymnesiophyceae, and Sagenista in the photic zone and DCM, transitioning to Radiolaria (Polycystinea and RAD-B) and Diplonemea in the aphotic zone (Fig. 3D). Dinophyceae and Prymnesiophyceae are common in pelagic waters, including in the GOM (*36*, *53*), and occupy important functional roles as grazers (and mixotrophs) in microbial food webs (fig. S5). Sagenista was also abundant in the photic zone (Fig. 3D), a group of common, yet still uncultured heterotrophic protists that have important ecological roles (*54*). Other class level protist groups that were common in the GOM in summer–fall, like Mamiellophyceae (Chlorophyta) and Mediophyceae (Stramenopiles), varied more greatly across transects in the photic zone and DCM (Fig. 3D). Radiolarians dominated relative abundance in mesopelagic samples (Fig. 3D). While these organisms remain largely uncultivated and hard to study, they are key members of deep ocean food webs, forming endosymbiotic relationships with other microorganisms (fig. S5) and contributing to the export of carbon and biogenic silica (*55*).

DNA metabarcoding also reinforced the importance of obligate parasites within the group Syndiniales at all depths in the water column (*42*, *56*, *57*), including at the basin scale in the GOM (Fig. 3D; fig. S5). The prevalence of Syndiniales may be attributed to their wide host range, active (and passive) export on sinking particles, and depth related niche partitioning (*56*, *58*). We observed vertical shifts within Syndiniales at the clade level in our samples that aligned with prior observations (*45*, *56*). For instance, there was a shift from Syndiniales Group-I Clades 1 and 4 in the photic zone to other clades, like Group-II Clade 7 and Group-I Clade 2 in the aphotic zone (fig. S8). Radiolaria also varied between clusters, with certain members of Polycystinea (e.g., *Heliosphaera* and *Pterocorys*) increasing in relative abundance from the DCM to the aphotic zone (fig. S8). Diplonemea were also dominant in the GOM aphotic zone (Fig. 3D). Though enigmatic, Diplonemea have been found globally in mesopelagic waters (*57*) and likely represent important consumers of picoplankton and bacteria in these environments (*59*).

Generalized linear models reveal group-specific environmental correlates

We used generalized linear models (GLMs) with either Poisson or negative-binomial error distributions to identify potential explanatory variables of major 16S and 18S taxonomic groups in the GOM. GLMs account for multiple predictor variables (factors) and have been applied to ecological count (and proportional) data of higher trophic level marine organisms (*60*, *61*). Here, we applied GLMs to microbial metabarcoding data, allowing us to observe predictor variables and their relation to group-specific relative abundance measured spatially in the photic zone (Fig. 2D; Fig. 3D). We focused our models on the photic zone (Cluster 1), primarily because most factors were collinear in the DCM and aphotic zone (table S1). Collinearity among variables can result in models being less statistically reliable and confound model interpretation (*62*). Eight of fifteen environmental variables were initially selected for models and included temperature, salinity, dissolved oxygen (O_2), nitrate (NO_3), ammonium (NH_4), phosphate (PO_4), dissolved inorganic carbon (DIC), and total pH recalculated to in situ temperatures (Table 1). Many parameters related to OA that were measured or derived (e.g., total alkalinity, pCO_2, carbonate ion concentration, and aragonite saturation) were strongly collinear to each other and temperature (Spearman $r_s > 0.7$ or < -0.7), and thus were excluded from initial models (table S1). Environmental conditions in the GOM surface were typical for this time of year (*63*, *64*). For instance, offshore waters were warm (> 28 °C) and nutrient-limited (e.g., $NO_3 < 0.1$ µmol kg^{-1}), while coastal regions had higher nutrient concentrations, including near the Mississippi River outflow (Table 1; fig. S2). DIC was highest in the southern GOM and onto the Campeche Bank (> 2050 µmol kg^{-1}), while pH often increased from the shelf to open ocean regions of the Gulf (Table 1; fig. S2).

Microbial groups differed in the type and number of variables that significantly contributed to the final models (Table 2). Pseudo R^2 values produced from GLMs ranged from 0.26–0.80

(Table 2), though several other methods confirmed appropriate model fit. First, model simulations fit the data well (Fig. 4C; Fig. 5C) and the standardized residuals were normally distributed for all groups (Kolmogorov–Smirnov, $P > 0.05$), except for Flavobacteriales. This was further supported by significant and often strong positive correlations (Pearson $R = 0.31$–0.90; $P < 0.01$) between test and model-trained relative abundance data for all groups (fig. S9; fig. S10), with example plots shown for SAR11 (Fig. 4D) and Syndiniales (Fig. 5D). Explanatory variables like temperature, DIC, and pH had individual, and often significant ($P < 0.05$) effects on relative abundance that varied among major 16S (Fig. 4A–B) and 18S groups (Fig. 5A–B). Through this approach, we examined individual model terms, focusing primarily on those related to ocean change, and explored their relationships with group-specific relative abundances in the GOM.

Our model findings often supported prior physiological responses for certain microbial groups that have been revealed in field and culture experiments. While changes in relative abundance data with any given environmental factor does not necessarily translate to physiology, applying DNA metabarcoding to OA research can help to verify existing trends and produce new hypotheses for future testing on a wide range of microorganisms (*22*, *23*). We found that temperature had a positive effect on the relative abundance of SAR11 and SAR86 in our models (Fig. 4A–B). Experimental evidence suggests that warmer conditions may favor increased biomass of small, oligotrophic bacteria, like SAR11 and SAR86, that have low nucleic acid content (*65*). In general, warming is thought to promote increased bacterial production, biomass, and respiration, while also lowering growth gross efficiency (*20*). DIC had a positive effect on SAR11, SAR86, and Flavobacteriales in group models (Fig. 4A–B), which together with temperature effects, may imply a favorable response among these taxa to continued OA and warming in this region. It is important to note that heterotrophic bacteria will also be influenced by indirect changes in plankton composition, dissolved organic matter (DOM) availability and quality, and trophic interactions (*21*, *66*). These factors may outweigh direct OA effects in natural communities and will be important to incorporate into future climate model predictions of bacterial diversity and composition.

We observed contrasting effects of pH on the relative abundance of *Prochlorococcus* vs. *Synechococcus* in the photic zone (Fig. 4A–B). For example, in situ pH had a strong and positive effect on *Prochlorococcus*, implying a negative response to lower pH (more acidic) conditions. An opposite trend was observed for pH in the *Synechococcus* model (Fig. 4A–B); however, DIC also had a negative effect on *Synechococcus*, confounding model inference. Fu et al. (2007) noted that combined effects of high pCO_2 and temperature significantly increased growth rates, photosynthetic capacity, and cellular pigment levels of *Synechococcus* but not *Prochlorococcus*. Mesocosm work in the subtropical North Atlantic also indicated a positive response of *Synechococcus* to high pCO_2 (*67*), though others have noted small or insignificant physiological shifts to changing conditions (*68*). On a global scale, ecological niche models predict increased *Prochlorococcus* and *Synechococcus* biomass to ocean warming (via flow cytometry),

275 particularly in low latitude regions like the GOM, where these taxa already dominate plankton
276 biomass (*69*). Such niche models have not considered pH (or DIC), which we show may be
277 significant predictors. Though not resolved at the ecotype level in our amplicon dataset,
278 individual cyanobacterial strains or ecotypes will likely respond differently to future conditions,
279 as well as be influenced by indirect changes in top-down pressure (grazing or viral lysis),
280 nutrients, or sunlight (*70*, *71*). Multiple ecotypes have already been discovered for
281 *Prochlorococcus* in the ocean, with evidence of different nutrient uptake rates, light preferences,
282 and thermal optima that shape population dynamics (*51*, *72*). Additional field and laboratory
283 work is needed to identify responses among microbes at the species or ecotype level to support
284 accurate model predictions (*13*) and reveal underlying physiological mechanisms.
285
286 Future OA and warming is predicted to favor small phytoplankton, like picoeukaryotes, that can
287 more efficiently exploit oligotrophic and nutrient-limited waters (*11*, *12*, *14*), primarily due to
288 their larger cell surface to volume ratios that promote resource acquisition. Though for many
289 protists, the effects of OA and warming are less clear. This is especially true for Syndiniales and
290 Sagenista, enigmatic protist parasites and grazers that have seldom been considered with respect
291 to climate change. In our models, temperature had a significant and positive effect on the relative
292 abundance of Syndiniales and Sagenista (Fig. 5A–B). Temperature is often thought to enhance
293 physiological rates (*73*), which may include microzooplankton grazing and parasitism; however,
294 temperature relationships are hard to predict and can often be confounded by other factors, like
295 host or prey composition, that can dictate mortality rates. We found that pH had a positive effect
296 on Syndiniales and Sagenista, while DIC had a negative impact on Syndiniales relative
297 abundance (Fig. 5A–B). This implied a negative response among these groups to more acidic
298 conditions in the GOM at this time. Therefore, models that include only temperature or pH may
299 result in different outcomes for certain plankton groups (*74*), potentially misleading how we
300 interpret (and predict) their responses to climate change.
301
302 Dinophyceae were also prevalent in the photic zone on GOMECC-4 (Fig. 3D). It is well
303 understood that dinoflagellates are central to the microbial loop in oligotrophic regions, often
304 exhibiting mixotrophy and representing a key link between primary production and higher
305 trophic levels (*29*, *53*). We found that temperature and DIC had significant and negative effects
306 on Dinophyceae relative abundance (Fig. 5A–B), implying a negative response to warmer and/or
307 more acidic conditions in the GOM. Similar findings on dinoflagellates have been observed in a
308 mesocosm study (*67*), though others have found dinoflagellates to benefit from or be less
309 sensitive to warming or increased pCO_2 concentrations (*23*, *71*, *74*, *75*). Dinoflagellates often
310 exhibit mixotrophy, and so favorable responses to OA among this group may be indicative of
311 increased consumption of common prey (picoeukaryotes and cyanobacteria) that tend to grow
312 faster under such conditions (*75*). As is the case with many protists, dinoflagellates are extremely
313 diverse, not only phylogenetically but also in terms of their size, physiology, and trophic modes
314 (*76*). Therefore, it will likely be challenging to define a unified response for Dinophyceae to
315 changing ocean conditions. Future work that merges DNA metabarcoding with more targeted

316 approaches, like single-cell genomics or qPCR, will help to shed light on species sensitivity,
317 interactions, and drivers that would otherwise be overlooked.
318
319 In addition to temperature and carbonate chemistry parameters, other factors like nutrients,
320 salinity, and oxygen had significant effects on prominent 16S and 18S groups in the GOM (Fig.
321 4A; Fig. 5A). As an example, limiting nutrients like NO_3 and PO_4 had negative effects on the
322 relative abundance of *Synechococcus* and *Prochlorococcus*, respectively (Fig. 4A). This may be
323 related to the ability of cyanobacteria to uptake nutrients at low concentrations in surface waters
324 (*72*). *Synechococcus* are thought to exploit low NO_3 concentrations in the GOM by maintaining a
325 shallower distribution in the water column (*64*), relying on regenerated sources of NO_3 via
326 nitrification (*29*). Salinity was also an important variable in our models, with positive effects on
327 the relative abundance of *Prochlorococcus*, Syndiniales, Dinophyceae, and Prymnesiophyceae,
328 as well as a negative effect on Flavobacteriales (Fig. 4A; Fig. 5A). Salinity is a known driver of
329 bacterial and plankton distribution and diversity in the GOM (*37*, *39*, *77*). This is particularly
330 evident in the northern GOM, where plankton biomass and composition are often driven by
331 salinity-induced stratification (and nutrient availability) that result from riverine discharge via
332 the Mississippi–Atchafalaya system, as well as by climatic processes, like the El Niño–Southern
333 Oscillation (*77*, *78*). Here, interpreting the role of salinity or nutrients in driving specific
334 microbial groups was difficult, mainly because our sampling strategy and analysis focused on
335 large-scale spatial patterns in microbial communities that did not allow us to explore regional
336 trends (e.g., in the northern GOM). Even so, our results emphasize the importance of including
337 such variables to resolve microbial composition and distribution at the basin scale in the GOM.
338
339 There are several caveats to consider with our model analysis. Models constructed from
340 amplicon data on GOMECC-4 reflected only a specific time of the year (summer–fall) and did
341 not integrate seasonal sampling. Temperature and carbonate chemistry parameters vary
342 seasonally in the GOM (*79*), as does the intensity and position of the Loop Current (and eddies)
343 and nutrient input from coastal runoff, all of which will impact microbial communities (*80*, *81*).
344 Consistent temporal sampling will be essential to better resolve microbes and their drivers over
345 seasonal and interannual time scales (*24*). Such sustained sampling will also allow for more
346 accurate predictions of microbial dynamics that integrate new OA data beyond the limits of
347 GOMECC-4 measurements. We also considered GLMs for major taxonomic groups that were
348 present in our samples (i.e., highest relative abundance), mainly to avoid issues with zero-
349 inflation and overdispersion in the models. As a result, several groups thought to be sensitive to
350 ocean change, like diatoms and diazotrophic cyanobacteria (*8*), were not considered here due to
351 lower relative abundance at the basin scale. Similarly, this constrained our ability to predict
352 model effects below the order to class level, with the exception being highly abundant
353 cyanobacterial genera. We examined linear trends with GLMs as a simple and conservative
354 approach to model relative abundance in the GOM. Future work may consider applying
355 generalized additive models (GAMs) that allow for nonlinear dynamics (*82*), especially as more
356 amplicon data is collected.

Though we tested for model fit, it is important to note that amplicon data is compositional, with relative abundance of any single group being dependent on the proportion of others (*83*). Comparing relative abundance among eukaryotic groups is also tenuous, as 18S rRNA gene copy numbers can vary greatly (2–166 copies per cell) among protists (*84*). This is especially true for alveolates (Syndiniales and Dinophyceae) and can lead to overestimation of read counts and relative abundance (*42*). However, such concerns would not necessarily discount our modeling approach that focused on groups separately and explored their relation to environmental factors. Lastly, models did not account for trophic interactions (e.g., changes in prey or host) that may vary along with changing conditions (*19*) or potential evolutionary adaptations among organisms (*85*). Nevertheless, applying GLMs to amplicon data in this study offered a first step to define multiple environmental drivers of diverse marine microbes, many of which are not easily discerned with traditional observational methods like microscopy or cytometry. Our findings are also timely for marine regions like the GOM that have lacked basin-scale sampling.

GLMs expand microbial distributions in GOM surface waters

Final models were used to predict the relative abundance of major 16S and 18S groups at 135 surface sites on GOMECC-4 (Fig. 1A), including 84 sites where DNA was not collected. This allowed us to increase the spatial resolution of microbial sampling in the GOM at this time of year. Groups like SAR11 (Fig. 6A) and Syndiniales (Fig. 6F) were well distributed throughout the GOM, with highest relative abundance predicted offshore of Brownsville (Texas), in the Bay of Campeche, and regions on the Campeche Bank. Cyanobacteria genera were largely partitioned in the GOM based on their expected ecological niches (*86*). *Prochlorococcus* was most relatively abundant offshore in stratified and nutrient-limited waters (Fig. 6B), particularly in parts of the southern GOM. *Synechococcus* was present throughout the GOM at the surface, but relative abundance was often highest in nutrient-rich coastal regions and in a localized area in the central Gulf (Fig. 6C). Other groups like SAR86 (Fig. 6D), Prymnesiophyceae (Fig. 6H), and Sagenista (Fig. 6I) were most relatively abundant offshore in the southern GOM and onto the East Mexico Shelf, likely driven by higher temperature and DIC concentrations in these areas (fig. S2). This was supported in the model output for these taxa, where temperature and/or DIC had positive effects on relative abundance (Fig. 4A; Fig. 5A). Flavobacteriales was highest near the Mississippi River outflow (Fig. 6E), in line with strong negative effects of salinity in the model output for this group (Fig. 4A). The Mississippi River is the dominant source of freshwater into the GOM, providing nutrients and organic matter into the system (fig. S2) that can stimulate phytoplankton blooms (*81*). Though not widespread in the GOM, diatoms were most relatively abundant in the photic zone near the Mississippi River (Fig. 3D), which may have contributed to higher relative abundance of copiotrophs like Flavobacteriales that often associate with blooms and can rapidly consume DOM (*87*).

Current predictions also revealed insights into the biogeography of a HAB species in the GOM. Though prevalent through most of the GOM, including in the open ocean, relative abundance of Dinophyceae was predicted to be highest directly off the coast of Tampa, Florida (Fig. 6G). This was caused by a likely bloom event of the mixotrophic dinoflagellate, *Karenia brevis*, captured in our DNA samples (fig. S11) and confirmed to be highly abundant through manual counts (10^5–10^6 cells l^{-1}) estimated around the same time and location via the Florida Fish and Wildlife Conservation Commission (https://myfwc.com/research/redtide/monitoring). HABs formed by *K. brevis* are common in the GOM in the summer–fall, particularly along the West Florida Shelf, and can negatively impact marine ecosystems and local economies (*32*, *33*, *35*). There is evidence that warming may increase toxin production, growth rates, bloom frequency, and range expansion of some HAB species (*88*). Temperature had negative effects on Dinophyceae in our models (Fig. 5A–B), but responses were not explored to genus level. In culture, *K. brevis* has shown increased growth rates with increasing pCO_2, though changes in toxin production were not recorded (*89*). It remains important to monitor HABs and their drivers (*90*), combining traditional monitoring and molecular methods to better predict pervasive blooms in the GOM and elsewhere.

Indicator analysis reveals candidate microbial indicator taxa of OA

It is also important to determine specific microorganisms below the order to class level that may be indicative of different OA conditions in natural waters (*9*, *10*, *23*). To this end, we grouped samples in the photic zone (Cluster 1) based on TA:DIC ratios and examined microbial indicator taxa at the ASV level. The TA:DIC ratio is a well-used proxy for carbonate chemistry in the ocean, determining the buffering capacity against acidification (*79*, *91*). In general, lower TA:DIC ratios indicate poorly buffered waters, and so in our case, microbes that were more prevalent in lower TA:DIC samples may be candidate indicators of more acidic conditions in the GOM. TA:DIC ratios ranged from 1.1–1.2 in the photic zone, were not influenced by sampling transect, and were positively correlated with pH (Pearson $R = 0.71$; $P < 0.01$) in surface waters (Fig. 7A–B). TA:DIC ratios were manually grouped into low (< 1.16) vs. high (> 1.16) categories to explore microbial indicators (Fig. 7A–B).

Overall, we found that 146 and 117 protist ASVs were significant indicators ($P < 0.001$) of low or high TA:DIC ratios, respectively (table S2). Protist indicators spanned a range of taxonomic groups, though several ASVs stood out (Fig. 7C). For instance, protists with the highest indicator values (> 0.35) in samples with low TA:DIC ratios included *Ostreococcus* sp., which was the most relatively abundant indicator ASV on average in the photic zone (~6%), as well as other ASVs assigned to *Emiliania huxleyi* (now *Gephyrocapsa huxleyi*), Cryptomonadales, *Euduboscquella* (Syndiniales), and Dino-Group I Clade 1 (Syndiniales). In comparison, ASVs with high indicator values (> 0.55) in samples with high TA:DIC ratios consisted of ASVs assigned to heterotrophic flagellates like MAST 3-B (and 4-B) and Kathablepharidida, as well as parasites in Dino-Group III and V (Fig. 7D). For 16S samples, a total of 228 and 136 ASVs were

438 significant indicators ($P < 0.001$) of low vs. high TA:DIC ratios (table S2), dominated by
439 Proteobacteria (fig. S12). 16S ASVs with the highest indicator values (> 0.45) in low TA:DIC
440 samples included an ASV assigned to SAR11 clade Ia, which accounted for 10% of reads on
441 average in Cluster 1, as well as other ASVs assigned to SAR11 (clade I and Ia), SAR406, and
442 AEGEAN-169 (fig. S12). The 16S ASVs that were most indicative of high TA:DIC were
443 assigned to SAR116, SAR86, AEGEAN-169, and Rickettsiales (family S25-593; fig. S12).
444
445 Pico- and nanoeukaryotes dominate warm and oligotrophic regions like the open GOM (*27*, *53*,
446 *64*) and are sensitive to changing ocean conditions (*15*, *23*). Two of arguably the most well
447 studied taxa in the field of phytoplankton OA research, *Ostreococcus* sp. and *Emiliania huxleyi*,
448 were associated with less buffered (and more acidic) waters in the GOM (Fig. 7C). Both species
449 are widespread and impact global biogeochemical cycles (*92*), with *E. huxleyi* being a major
450 calcifier and contributor to $CaCO_3$ flux (*93*). In a prior 18S rRNA metabarcoding survey in the
451 southern GOM, *Ostreococcus* was the only genus with significantly different relative abundance
452 between upwelling and downwelling conditions in the DCM and when comparing the DCM to
453 mixed layer (*38*), which authors suggest may make this species an indicator of vertical nitrate
454 flux. Our findings imply *Ostreococcus* may also be a candidate indicator of acidic conditions in
455 GOM surface waters. Calcifying plankton, like *E. huxleyi*, are thought to be strongly impacted by
456 OA, with increased pCO_2 and/or lower pH having detrimental effects on growth and calcification
457 rates (*15*, *16*). However, contrasting effects have been observed and may reflect considerable
458 strain and ecotype variability (*18*, *23*). Indeed, several culture-based studies with *E. huxleyi* (and
459 *Ostreococcu*s) have revealed adaptive mechanisms of cells to elevated pCO_2 over hundreds of
460 generations (*94*, *95*). Though *E. huxleyi* was not prevalent overall in our samples (fig. S8), this
461 species has been measured in high concentrations (~10^4 cells l^{-1}) in the southern GOM in spring
462 (*96*). Together with model results at the class level (positive temperature effects on
463 Prymnesiophyceae), our findings highlight the potential sensitivity of haptophytes to changing
464 conditions in the GOM that should be further explored.
465
466 Indicator analysis also revealed SAR11, specifically ASVs assigned to clades 1 and 1a, as being
467 possible indicators of less buffered waters in the GOM in summer–fall (fig. S12). SAR11 is the
468 most abundant bacterial group in the oceans, playing an important role in global carbon cycling
469 (*97*). Though diverse, members of the SAR11 clade Ia ecotype tend to be most prevalent in
470 surface oceans (*52*), adapted to nutrient-poor conditions via small cell sizes and streamlined
471 genomes (*98*). Though direct effects of OA on SAR11 remain unclear and are likely to be less
472 important compared to shifts in DOM (*21*), SAR11 exhibits known seasonality in the surface
473 oceans and is sensitive to temperature (*48*, *65*). Such temperature sensitivity was supported in
474 our model analysis (Fig. 4A–B). Given the ubiquity of SAR11 and its role in global carbon
475 cycles, it remains critical to confirm and further investigate the potential of this group as an
476 indicator of ocean change.
477

Future sampling to characterize microbes in changing oceans

Efforts to characterize microbial communities over natural physicochemical gradients are essential to inform how these communities may shift in the face of changing ocean conditions (*10*). In the GOM, there is evidence of increased pCO_2 in many parts of the open ocean that are on par with rates of change in other oligotrophic regions (*99*), like those measured in the Pacific Ocean via the Hawaiian Ocean Time-series (1.72 $\mu atm\ yr^{-1}$) and in the Atlantic Ocean via the Bermuda Atlantic Time-series Study (1.69 $\mu atm\ yr^{-1}$). Yet, knowledge on the effects of OA and warming on biological organisms is limited in the GOM, particularly for microbes. Here, we performed the first basin-scale DNA metabarcoding survey in the GOM and paired this with extensive hydrographic, nutrient, and carbonate chemistry measurements to investigate diverse prokaryotes and protists and their specific environmental drivers (Fig. 1). In line with prior physiological and modeling-based observations, our GOM model analyses suggest that more acidic and warmer conditions in the GOM may favor heterotrophic bacteria (SAR11 and SAR86) and smaller phytoplankton (e.g., Prymnesiophyceae), with groups like Dinophyceae potentially being less favored in future conditions (Fig. 4; Fig. 5). Warming and OA in the GOM may have contrasting effects on major plankton parasites (Syndiniales) and grazers (Sagenista) that are seldom considered with respect to climate change and underscores the importance to measure multiple stressors simultaneously (Fig. 5). We also defined microbial indicator taxa at the ASV level (Fig. 7), which resulted in several ubiquitous (and environmentally sensitive) microbes, like *Ostreococcus* sp., *Emiliania huxleyi*, and SAR11 clade Ia, being associated with more acidic waters in the GOM. Model inference and the utility of identified ASVs to act as indicator species of OA will need to be further tested, including at different times of the year to reflect seasonal turnover of the microbial community.

Though still unclear, empirical and predictive work suggests that changes in our ocean systems will likely have profound impacts on microbial composition, biogeography, and physiology (*8*, *100*), with consequences for trophic transfer, nutrient cycling, and carbon export. Global models and experimental evidence predict increased stratification with warming, shifting communities to smaller picophytoplankton that can better exploit nutrients and other resources (*12*, *14*). Warming-induced stratification may also result in an overall net reduction in carbon export that may threaten to decrease the amount of organic carbon that reaches the seafloor (*101*). Yet, predicted shifts in carbon export in global ecosystem models remains uncertain, ranging from a 41% decrease to 8% increase in carbon export flux in future oceans (*102*). Strong selection imposed by climate change may also drive rapid adaptation, competition, or the emergence of new species (e.g., with higher thermal tolerance), all restructuring microbial communities (*8*, *13*, *85*). In culture, some microbes demonstrate the ability to adapt to warmer or more acidic conditions (*94*, *95*), though this does not necessarily mean they will remain competitive and it remains an open question on how this will apply to natural systems with mixed assemblages (*19*, *85*). Further, current models do not fully account for trophic interactions, like grazing or parasitism, the rates of which will likely vary in future oceans and offset direct physiological

effects of OA or warming on certain microbes. It remains important to measure microbial interactions, plankton mortality rates, and carbon export rates over time and in space (*10*, *102*), which will support a more mechanistic approach to model predictions.

Our findings provide an important baseline for microbial OA research in the GOM; however, sampling on GOMECC-4 only reflected a single time of the year and did not consider known seasonal variability in carbonate chemistry parameters or hydrography (*79*, *80*), which are likely to influence microbes and their drivers (*36*). In response, there is a need for sustained biological measurements in the GOM, either by establishing long-term monitoring programs or continuing to leverage existing oceanographic surveys, like GOMECC. Long term microbial sampling in the GOM will be essential to accurately predict future changes in microbial groups that may be expected with continued OA or warming. For example, increased DNA collection would support ecosystem modeling of microbes in the GOM, integrating climate model scenarios (e.g., via the Coupled Model Intercomparison Project) to predict shifts in microbial abundance by the end of the century. Ultimately, our ability to predict the response of marine microbes to climate change will depend on sustained and coordinated sampling efforts across a range of dynamic marine ecosystems.

Materials and Methods

Seawater collection, DNA filtration, and environmental metadata

Seawater was collected on board the NOAA Ship *Ronald H. Brown* as part of GOMECC-4 from September 13 to October 21, 2021. Sampling for GOMECC-4 occurred along 16 inshore–offshore transects across the entire GOM and an additional line at 27°N latitude in the Atlantic Ocean (Fig. 1A). Sampling started at the 27°N line and continued counterclockwise across the GOM, ending at Florida Straits and Cape Coral. We also collected DNA samples near Padre Island National Seashore (U.S. National Parks Service), a barrier island located off the coast of south Texas (Fig. 1A). Vertical CTD sampling was employed at each site to measure discrete physical, chemical, and biological properties. Water sampling for DNA filtration was conducted at 51 out of 141 total sites and three depths per site, representing the surface, deep chlorophyll maximum (DCM), and near bottom (fig. S1).

At each respective site and depth, seawater was collected from pre-designated Niskin bottles on a CTD rosette. To ensure adequate amounts of water were filtered for DNA analysis, samples for chemical parameters were taken at the same depths but with different discrete Niskin bottles. Following a CTD cast, which varied in duration from 30 min to 3 h depending on water depth, whole seawater was transferred from Niskin bottles to triplicate Whirl-Pak bags (3 depths x 3 replicates = 9 bags per site). Within an hour, whole seawater (~2 L per replicate) was filtered through 0.22-µm Sterivex filters (Millipore; CAT# SVGP01050) via a peristaltic pump (100–150 rpm) and run dry. Filters were capped and outlets were sealed with parafilm. Filters were stored

559 at –80 °C on the ship and kept at the same temperature in the laboratory for longer-term storage.
560 Filter lines were sterilized with 2% bleach and rinsed with Milli-Q after every site. Milli-Q
561 blanks were also filtered randomly throughout the duration of the cruise. Accounting for blanks
562 and replication, a total of 481 Sterivex filters were collected on GOMECC-4.
563
564 Discrete samples for water column hydrography and chemistry were taken at each site and depth
565 during GOMECC-4, including sites sampled for DNA. Temperature, salinity, pressure, and
566 chlorophyll fluorescence were obtained from the CTD. Vertical CTD profiles on the downcast
567 were used to estimate the position of the DCM at each site. Blanks and quality control samples
568 were considered for each discrete chemical parameter. Dissolved oxygen concentration was
569 estimated from water samples (125 ml) using an automated oxygen titrator with amperometric
570 end-point detection (*103*). Nutrient samples were collected from Niskin bottles into 50-ml acid
571 washed bottles. Dissolved nutrients (NO_3, NO_2, NH_4, PO_4, and SiO_4) were measured on board
572 using an automated continuous flow analytical system with colorimetric detection ((*104*); SEAL
573 Analytical). Samples for DIC were collected from Niskin bottles into 294-ml borosilicate glass
574 bottles, sealed with glass stoppers, and stored for 12 h at room temperature. DIC samples were
575 analyzed on the ship using two analytical systems, each consisting of a coulometer (CM5017,
576 UIC Inc.) coupled with a Dissolved Inorganic Carbon Extractor (*105*).
577
578 Samples for total alkalinity (TA) were collected from Niskin bottles into 500-ml collection
579 bottles, preserved with a mercuric chloride solution, and kept in a water bath at 22 ºC for 1 h
580 prior to analysis. TA measurements were made using a two-titration system, consisting of a
581 Metrohm 765 or 665 Dosimat Titrator and Orion 720A or 2-Star pH meter (*106*). Samples for
582 pCO_2 were drawn from Niskin bottles into 500-ml glass bottles, preserved with mercuric
583 chloride, and stored at room temperature for 8 h before analysis. Details on the system used to
584 measure pCO_2 are described in (*107*) and include equilibrating each sample with a constantly
585 circulating gas phase. Lastly, for pH analysis, samples were collected from Niskin bottles into
586 10-cm (~30 ml) glass cylindrical optical cells and analyzed on an Agilent 8453
587 spectrophotometer with a custom-made temperature-controlled cell holder (*108*). Aragonite
588 saturation state was calculated at each site and depth based on temperature, salinity, pressure,
589 DIC, and TA using the CO2SYS program for CO_2 System Calculations (*109*). Measurements of
590 pCO_2 (20 ºC) and pH (25 ºC) were re-calculated to in situ conditions using pressure, temperature,
591 salinity, DIC, and TA in CO2SYS (*109*). Environmental metadata associated with DNA samples
592 are provided in table S3.
593
594 **DNA extractions, PCRs, and library preparations**
595
596 Sterivex filters were extracted in-house at NOAA's Atlantic Oceanographic and Meteorological
597 Laboratory (AOML) using the ZymoBIOMICS 96 DNA/RNA MagBead kit (Zymo; CAT#
598 D4308), with modifications for in-cartridge bead beating as described in (*110*). Filters were
599 thawed, the inlet caps were removed, and excess water was dried from the inlet using kimwipes

600 to allow for dispensing of beads into the cartridge. Premade mixtures of 0.1 mm and 0.5 mm
601 beads were directly added into the filters to ensure adequate lysis and recovery of hard-to-lyse
602 phytoplankton groups (*110*). This was followed by the addition of a lysis buffer (1 ml). Sterivex
603 filters were vortexed for 40 min on a Vortex-Genie at maximum speed (~3200 rpm). DNA
604 lysates were transferred to 2-ml LoBind tubes (Eppendorf) via syringe and centrifuged for 1 min
605 at 10,000 g. Supernatant (750 µl per sample) was split across three KingFisher 96-well plates
606 (250 µl per plate). Zymo MagBinding buffer (600 µl) and magnetic beads (25 µl) were added to
607 each well in each of the three plates. With this setup, 96 samples were extracted at the same time
608 on the automated KingFisher Flex (Thermo Fisher). Each run included three wash plates with
609 500–900 µl per well of MagWash and an elution plate with 150 µl per well of molecular-grade
610 water. DNA was eluted into a single well from the same discrete sample across replicate plates.
611 Concentrations of eluted DNA were measured using a Varioskan LUX plate reader and the
612 Quant-IT dsDNA Assay (Thermo Fisher) and corrected per replicate sample based on volume of
613 seawater filtered (ng l^{-1}; fig. S13). Filters were processed randomly. Extraction blanks (clean
614 Sterivex filters) were also included and processed similarly. A bacterial mock community
615 (Zymo) was included as a positive control.
616
617 Metabarcoding libraries were initially prepared at AOML, amplifying DNA of target organisms
618 with universal primers, including 16S (Bacteria and Archaea) and 18S rRNA (protists). Primers
619 from (*111*) were used to target the 16S V4–V5 region: forward (515f; 5'-
620 GTGYCAGCMGCCGCGGTAA-3') and reverse (926r; 5'-CCGYCAATTYMTTTRAGTTT-
621 3'). Primers from (*112*) and the Earth Microbiome Project
622 (http://www.earthmicrobiome.org/emp-standard-protocols/18s/) targeted the 18S V9 region:
623 forward (1391f; 5'-GTACACACCGCCCGTC-3') and reverse (EukBr; 5'-
624 TGATCCTTCTGCAGGTTCACCTAC-3'). Primers were constructed with Fluidigm common
625 oligos CS1 forward (CS1-TS-F: 5'-ACACTGACGACATGGTTCTACA-3') and CS2 reverse
626 (CS2-TS-R: 5'-TACGGTAGCAGAGACTTGGTCT-3') fused to their 5' ends, to enable two-
627 step library preparation at the Michigan State University Research Technology Support Facility
628 (RTSF).
629
630 PCR reactions were run in triplicate (12.5 µl per sample), with 1 µl of DNA per sample. 16S
631 PCR reactions consisted of 5 µl of AmpliTaq Gold, 6.25 µl of water, and 0.375 µl of each primer
632 (10 µM); PCR conditions included denaturation at 95 °C for 2 min, 25 cycles of 95 °C for 45 s,
633 50 °C for 45 s, and 68 °C for 90 s, followed by a final elongation step of 68 °C for 5 min (*111*).
634 18S PCR reactions consisted of 5 µl of AmpliTaq Gold, 6.5 µl of water, and 0.25 µl of each
635 primer (10 µM); PCR reactions involved denaturation at 94 °C for 3 min, 35 cycles of 94 °C for
636 45 s, 65 °C for 15 s, 57 °C for 30 s, and 72 °C for 90 s, followed by a final elongation step of 72
637 °C for 10 min (*112*). PCR products were pooled and run on a 2% agarose gel to confirm
638 amplification of target bands. Sample plates were submitted to the Michigan State University
639 RTSF Genomics Core for secondary PCR and sequencing.
640

641 Secondary PCR used dual-indexed, Illumina-compatible primers, targeting the Fluidigm
642 CS1/CS2 oligomers at the ends of the PCR products. PCR conditions for the secondary run
643 included an initial denaturation step at 95 °C for 3 min, 11 cycles of 95 °C for 15 s, 60 °C for 30
644 s, and 72 °C for 60 s, followed by elongation at 72 °C for 3 min. Amplicons were batch
645 normalized using Invitrogen SequalPrep DNA Normalization plates and the recovered product
646 was pooled. The pool was QC'd and quantified using a combination of Qubit dsDNA HS,
647 Agilent 4200 TapeStation HS DNA1000, and Invitrogen Collibri Library Quantification qPCR
648 assays. The RTSF Core included a sequencing blank for each sample plate. Separate sequencing
649 runs were performed using an Illumina MiSeq (2 × 250 bp) for 18S and 16S samples. Custom
650 sequencing and index primers complementary to the Fluidigm CS1 and CS2 oligomers were
651 added to appropriate wells of the reagent cartridge. Base calling was done by Illumina Real Time
652 Analysis (RTA) v1.18.54 and output of RTA was demultiplexed and converted to FASTQ
653 format with Illumina Bcl2fastq v2.20.0.
654
655 **Bioinformatics and functional assignments**
656
657 Primers were removed from demultiplexed FASTQ sequences using Cutadapt (*113*). Trimmed
658 reads were processed in Tourmaline, which implements QIIME 2 (and DADA2 plugins) in a
659 Snakemake workflow (*114*). Paired-end DADA2 was used to infer 16S and 18S amplicon
660 sequence variants or ASVs (*115*). Taxonomic assignments were also performed in Tourmaline
661 using reference files from SILVA (Version 138.1; (*116*)) and the Protistan Ribosomal Reference
662 or PR2 (Version 5.0.1; (*117*)) databases for 16S and 18S ASVs, respectively. In both cases,
663 taxonomy was assigned using a Naïve Bayes classifier trained to the respective databases and
664 trimmed to the primer regions (*118*). Output files (taxonomy, count, and metadata) were
665 imported separately into R (Version 4.3.1) using qiime2R (Version 0.99.6;
666 https://github.com/jbisanz/qiime2R) and merged with phyloseq (Version 1.44.0; (*119*)). Several
667 groups were removed from the 18S dataset: Metazoa, Streptophyta, Rhodophyta, and unassigned
668 reads at the Subdivision level. 18S reads assigned to non-marine taxa, e.g., Insecta, Archosauria,
669 and Ascomycota were also filtered out. For 16S, reads assigned to Chloroplast, Mitochondria,
670 and Eukaryota were removed. Samples with less than 3,000 reads counts were filtered out for
671 18S (5,000 reads for 16S), along with ASVs only observed once in each respective dataset.
672 Species accumulation curves were generated for 18S and 16S samples using the R package
673 ranacapa (Version 0.1.0; (*120*)). The number of reads vs. ASVs was saturated with respect to
674 categorial depth and position of samples on the shelf vs. open GOM, indicating that an
675 appropriate sequencing depth was reached (fig. S14). Samples were rarefied to the minimum
676 read count to normalize for differences in library size.
677
678 Protist ASVs were manually assigned to functional groups based on 18S V9 functional
679 annotations (https://doi.org/10.5281/zenodo.3768950) that were previously applied to Tara
680 Ocean communities (*57*). Additional databases (e.g., World Register of Marine Species) and
681 literature searches were also used. The following functional groups were included for 18S

682 protists: autotrophic protists, heterotrophic protists, mixotrophic protists, parasites,
683 photosymbionts, and other protists. Mixotrophic protists were further categorized as being
684 constitutive mixotrophs (CM) that inherently have chloroplasts and endosymbiotic specialist
685 non-constitutive mixotrophs (eSNCM) that harbor endosymbionts to support growth (*121*). We
686 recognize that many protists likely exhibit mixotrophy in some capacity, and so, our functional
687 annotation of this group may be underrepresented. Other protists represented higher level
688 taxonomic groups (domain or supergroup) that were unassigned at lower levels. Bacteria and
689 Archaea were categorized functionally as being heterotrophic or autotrophic.
690
691 **Statistical analyses**
692
693 Prior to ordination, ASV count tables were transformed to Aitchison distances, which is
694 estimated by transforming read counts via centered log-ratio normalization and computing
695 Euclidean distances. The resulting Aitchison distance matrices were used to observe microbial
696 composition and aimed to minimize compositional bias inherent with amplicon data (*83*).
697 Principal coordinate analysis (PCoA) of Aitchison distances was used to visualize 16S and 18S
698 community composition. Permutational multivariate analysis of variance (PERMANOVA) tests
699 were employed with the adonis2 function in vegan (9999 permutations) to estimate the impact of
700 spatial factors on community composition. This included categorical depth (surface, DCM, and
701 near bottom), sampling transect, and location of samples on the continental shelf vs. in open
702 ocean regions of the GOM designated by the 200 m isobath (Fig. 1A).
703
704 Samples were also grouped into clusters via hierarchical clustering (Ward's method) based on
705 Aitchison distances using the hclust function in vegan (Version 2.6-6.1; (*122*)). The optimal
706 number of clusters was determined based on average silhouette widths using the factoextra
707 package (Version 1.0.7; (*123*)). Silhouette widths offer an estimate on the quality of sample
708 clustering, with higher width coefficients indicating optimal clustering (*124*). Three clusters were
709 found to be optimal for both 16S and 18S (fig. S15), which largely reflected depth in the water
710 column (Fig. 1B; fig. S1). Cluster 1 consisted of samples collected at all depths on the shelf and
711 offshore in the surface layer, all confined to the photic zone (2–99 m). Cluster 2 consisted of
712 samples mainly from offshore and more stratified waters in the DCM (2–124 m), while Cluster 3
713 represented samples collected offshore in meso- to bathypelagic waters (135–3,326 m). The
714 photic zone extends to 200 m in many deeper regions of the GOM, and so, samples in Cluster 2
715 (and a handful in Cluster 3) were also technically collected within the photic zone. However, we
716 distinguish communities in Clusters 2–3 from Cluster 1 based on the large proportion of samples
717 confined to the open ocean DCM (Cluster 2; 80%) and mesopelagic (Cluster 3; 98%) that reflect
718 disparate habitats in the GOM.
719
720 Mean Shannon diversity index and richness (# of ASVs) were determined for each cluster using
721 the estimate_richness function in phyloseq (*119*) and compared against other clusters with
722 Wilcoxon tests ($P < 0.05$). Mean diversity and richness were also estimated along transects,

applying local regression (loess) curves to visualize trends using the geom_smooth function in ggplot2 (Version 3.5.1; (*125*)). Stacked bar plots displaying mean relative abundance were observed at the class level for 18S and order level for 16S for each sampling transect and cluster using the microeco package in R (Version 1.7.1; (*126*)). Taxonomic profiles were also observed using the treemap package in R (Version 2.4-4; (*127*)), a tiered approach to visualize relative abundance across multiple taxonomic levels.

Indicator taxa that were more abundant and representative of high (or low) TA:DIC ratios were statistically inferred using the indicspecies package in R (Version 1.7.14; (*128*)). The TA:DIC ratio was chosen because it is a good proxy to determine the ocean's capacity to absorb anthropogenic CO_2 by influencing its buffering capacity (*91*). Higher ratios indicate strong buffering capacity (i.e., the capacity of seawater to buffer against acidification). Based on histograms of TA:DIC, samples were grouped a priori into high (> 1.16) or low categories (< 1.16) that reflect different OA conditions (Fig. 7A–B). We focused on DNA samples collected from the photic zone (Cluster 1) to mitigate natural depth effects and to provide additional context to models (see next section). Indicator analysis was run separately on rarefied 16S or 18S samples that were agglomerated to the species level using the function multipatt with 999 permutations (*128*). Significant ASVs ($P < 0.001$) were retained and summarized for high (or low) TA:DIC and plotted against their mean relative abundance in the photic zone.

Generalized linear models

Generalized linear models (GLMs) were used to examine relationships between environmental factors (predictor variables) and the relative abundance of major microbial groups (response variables). GLMs focused on DNA samples collected in the photic zone (Cluster 1), in large part to mitigate collinearity of factors that was prevalent in Clusters 2–3 (table S1). Separate GLMs were performed for the top four most relatively abundant order level 16S and class level 18S groups (Table 2). Separate models were constructed for *Synechococcus* and *Prochlorococcus* to resolve differences between major cyanobacteria genera. Only variables that met requirements of low collinearity (Spearman $r_s < 0.7$ or > -0.7) and a variance inflation factor (VIF) < 10 were considered (*129*). Zurr et al. (2010) suggest using a more stringent VIF cutoff (< 3). However, we aimed to retain as many variables in the dataset as possible, which meant a few variables (e.g., DIC and salinity) approached VIF = 10. To select the best model for each 18S or 16S group, variables were further selected in a stepwise manner based on Akaike Information Criteria (AIC) values using the stepAIC function in the MASS package in R (Version 7.3-60; (*130*)). Only significant variables ($P < 0.05$) were used in the final model.

Final models were constructed with either Poisson or negative binomial error distributions. Initial model type was chosen by comparing standardized residuals and other model indices (e.g., AIC) with the compare_performance function in the performance package in R (Version 0.11.0; (*131*)). GLMs were implemented with the glm.nb function for negative binomial models in the

764 MASS package or the glm function for Poisson models (family = Poisson) in the stats package in
765 base R (Version 4.3.1). We observed overdispersion in relative abundance data for several
766 Poisson models (Syndiniales, Dinophyceae, *Synechococcus*, and *Prochlorococcus*), in which
767 case negative binomial models were applied (Table 2). Model quality and fit was estimated for
768 each group using the check_model function in the performance package (*131*), which included
769 plots of posterior predictive checks (model simulations), standardized residuals (Q–Q plots),
770 homogeneity of variance, and collinearity of selected predictor variables. The goodness of fit
771 was assessed with a pseudo R^2 (Nagelkerke's), though standardized residual checks of the final
772 models were also carried out (*62*) to assess model fit and uniformity of the residuals
773 (Kolmogorov–Smirnov, $P > 0.05$). As an additional validation, relative abundance data for each
774 group was randomly split and trained with respective models using 80% of the data to predict a
775 test set that was left out (20%). Pearson correlations were performed between model-trained and
776 test data.
777
778 Model coefficients were scaled and visualized for each 18S and 16S group using the multiplot
779 function in the coefplot package in R (Version 1.2.8; (*132*)). Individual factors were plotted
780 against predicted relative abundance using the plot_model function in the sjPlot package in R
781 (Version 2.8.16; (*133*)). We focused predictive plots on temperature and carbonate chemistry
782 parameters (DIC and pH). Group-specific GLMs were used to predict relative abundance at all
783 GOMECC-4 sites where surface layer (< 10 m) variables were collected (135 out of 141 sites).
784 Six stations did not have representative CTD data available at the surface layer and were
785 excluded. Predicted relative abundance for all surface GOMECC-4 sites were observed in Ocean
786 Data View using Data-Interpolating Variational Analysis (DIVA) interpolation (*134*).
787

References

1. S. Díaz, J. Fargione, F. S. Chapin 3rd, D. Tilman, Biodiversity loss threatens human well-being. *PLoS Biol.* **4**, e277 (2006).

2. N. Gruber, D. Clement, B. R. Carter, R. A. Feely, S. van Heuven, M. Hoppema, M. Ishii, R. M. Key, A. Kozyr, S. K. Lauvset, C. Lo Monaco, J. T. Mathis, A. Murata, A. Olsen, F. F. Perez, C. L. Sabine, T. Tanhua, R. Wanninkhof, The oceanic sink for anthropogenic CO2 from 1994 to 2007. *Science* **363**, 1193–1199 (2019).

3. S. C. Doney, D. S. Busch, S. R. Cooley, K. J. Kroeker, The Impacts of Ocean Acidification on Marine Ecosystems and Reliant Human Communities. *Annu. Rev. Environ. Resour.* **45**, 1–30 (2020).

4. J. C. Orr, V. J. Fabry, O. Aumont, L. Bopp, S. C. Doney, R. A. Feely, A. Gnanadesikan, N. Gruber, A. Ishida, F. Joos, R. M. Key, K. Lindsay, E. Maier-Reimer, R. Matear, P. Monfray, A. Mouchet, R. G. Najjar, G.-K. Plattner, K. B. Rodgers, C. L. Sabine, J. L. Sarmiento, R. Schlitzer, R. D. Slater, I. J. Totterdell, M.-F. Weirig, Y. Yamanaka, A. Yool, Anthropogenic ocean acidification over the twenty-first century and its impact on calcifying organisms. *Nature* **437**, 681–686 (2005).

5. M. M. White, D. C. McCorkle, L. S. Mullineaux, A. L. Cohen, Early exposure of bay scallops (*Argopecten irradians*) to high CO_2 causes a decrease in larval shell growth. *PLoS One* **8**, e61065 (2013).

6. R. K. Pachauri, M. R. Allen, V. R. Barros, J. Broome, W. Cramer, R. Christ, J. A. Church, L. Clarke, Q. Dahe, P. Dasgupta, N. K. Dubash, Climate Change 2014: Synthesis Report. Contribution of Working Groups I, II and III to the Fifth Assessment Report of the Intergovernmental Panel on Climate Change (IPCC, 2014).

7. A. Z. Worden, M. J. Follows, S. J. Giovannoni, S. Wilken, A. E. Zimmerman, P. J. Keeling, Rethinking the marine carbon cycle: Factoring in the multifarious lifestyles of microbes. *Science* **347**, 127594 (2015).

8. D. A. Hutchins, F. Fu, Microorganisms and ocean global change. *Nat Microbiol* **2**, 17058 (2017).

9. P. W. Boyd, D. A. Hutchins, Understanding the responses of ocean biota to a complex matrix of cumulative anthropogenic change. *Mar. Ecol. Prog. Ser.* **470**, 125–135 (2012).

10. D. A. Caron, D. A. Hutchins, The effects of changing climate on microzooplankton grazing and community structure: drivers, predictions and knowledge gaps. *J. Plankton Res.* **35**, 235–252 (2012).

11. D. G. Boyce, M. R. Lewis, B. Worm, Global phytoplankton decline over the past century. *Nature* **466**, 591– 596 (07 2010).

12. L. Bopp, L. Resplandy, J. C. Orr, S. C. Doney, J. P. Dunne, M. Gehlen, P. Halloran, C. Heinze, T. Ilyina, R. Séférian, J. Tjiputra, M. Vichi, Multiple stressors of ocean

ecosystems in the 21st century: projections with CMIP5 models. *Biogeosciences* **10**, 6225–6245 (2013).

13. S. Dutkiewicz, J. J. Morris, M. J. Follows, J. Scott, O. Levitan, S. T. Dyhrman, I. Berman-Frank, Impact of ocean acidification on the structure of future phytoplankton communities. *Nat. Clim. Chang.* **5**, 1002–1006 (2015).

14. S. A. Henson, B. B. Cael, S. R. Allen, S. Dutkiewicz, Future phytoplankton diversity in a changing climate. *Nat. Commun.* **12**, 5372 (2021).

15. K. R. M. Mackey, J. J. Morris, F. M. M. Morel, S. A. Kranz, Response of Photosynthesis to Ocean Acidification. *Oceanography* **28**, 74–91 (2015).

16. M. Segovia, M. R. Lorenzo, C. Iñiguez, C. García-Gómez, Physiological stress response associated with elevated CO2 and dissolved iron in a phytoplankton community dominated by the coccolithophore *Emiliania huxleyi*. *Mar. Ecol. Prog. Ser.* **586**, 73–89 (2018).

17. V. Vázquez, P. León, F. J. L. Gordillo, C. Jiménez, I. Concepción, K. Mackenzie, E. Bresnan, M. Segovia, High-CO2 Levels Rather than Acidification Restrict *Emiliania huxleyi* Growth and Performance. *Microb. Ecol.* **86**, 127–143 (2023).

18. M. D. Iglesias-Rodriguez, P. R. Halloran, R. E. M. Rickaby, I. R. Hall, E. Colmenero-Hidalgo, J. R. Gittins, D. R. H. Green, T. Tyrrell, S. J. Gibbs, P. von Dassow, E. Rehm, E. V. Armbrust, K. P. Boessenkool, Phytoplankton calcification in a high-CO2 world. *Science* **320**, 336–340 (2008).

19. A. C. Martiny, G. I. Hagstrom, T. DeVries, R. T. Letscher, G. L. Britten, C. A. Garcia, E. Galbraith, D. Karl, S. A. Levin, M. W. Lomas, A. R. Moreno, D. Talmy, W. Wang, K. Matsumoto, Marine phytoplankton resilience may moderate oligotrophic ecosystem responses and biogeochemical feedbacks to climate change. *Limnol. Oceanogr.* **67**, S378–S389 (2022).

20. H. Sarmento, J. M. Montoya, E. Vázquez-Domínguez, D. Vaqué, J. M. Gasol, Warming effects on marine microbial food web processes: how far can we go when it comes to predictions? *Philos. Trans. R. Soc. Lond. B Biol. Sci.* **365**, 2137–2149 (2010).

21. X. A. G. Morán, F. Baltar, C. Carreira, C. Lønborg, Responses of physiological groups of tropical heterotrophic bacteria to temperature and dissolved organic matter additions: food matters more than warming. *Environ. Microbiol.* **22**, 1930–1943 (2020).

22. T. E. Berry, B. J. Saunders, M. L. Coghlan, M. Stat, S. Jarman, A. J. Richardson, C. H. Davies, O. Berry, E. S. Harvey, M. Bunce, Marine environmental DNA biomonitoring reveals seasonal patterns in biodiversity and identifies ecosystem responses to anomalous climatic events. *PLoS Genet.* **15**, e1007943 (2019).

23. R. Gallego, E. Jacobs-Palmer, K. Cribari, R. P. Kelly, Environmental DNA metabarcoding reveals winners and losers of global change in coastal waters. *Proceedings of the Royal Society B* **287**, 20202424 (2020).

24. E. Osborne, X. Hu, E. R. Hall, K. Yates, J. Vreeland-Dawson, K. Shamberger, L. Barbero, J. Martin Hernandez-Ayon, F. A. Gomez, T. Hicks, Y.-Y. Xu, M. R. McCutcheon, M. Acquafredda, C. Chapa-Balcorta, O. Norzagaray, D. Pierrot, A. Munoz-Caravaca, K. L. Dobson, N. Williams, N. Rabalais, P. Dash, Ocean acidification in the Gulf of Mexico: Drivers, impacts, and unknowns. *Prog. Oceanogr.* **209**, 102882 (2022).

25. N. N. Rabalais, R. E. Turner, W. J. Wiseman Jr, Hypoxia in the Gulf of Mexico. *J. Environ. Qual.* **30**, 320–329 (2001).

26. W. Sturges, R. Leben, Frequency of Ring Separations from the Loop Current in the Gulf of Mexico: A Revised Estimate. *J. Phys. Oceanogr.* **30**, 1814–1819 (2000).

27. L. Linacre, R. Durazo, V. F. Camacho-Ibar, K. E. Selph, J. R. Lara-Lara, U. Mirabal-Gómez, C. Bazán-Guzmán, A. Lago-Lestón, E. M. Fernández-Martín, K. Sidón-Ceseña, Picoplankton carbon biomass assessments and distribution of *Prochlorococcus* ecotypes linked to loop current eddies during summer in the southern gulf of Mexico. *J. Geophys. Res. C: Oceans* **124**, 8342–8359 (2019).

28. T. T. Sutton, M. R. Clark, D. C. Dunn, P. N. Halpin, A. D. Rogers, J. Guinotte, S. J. Bograd, M. V. Angel, J. A. A. Perez, K. Wishner, R. L. Haedrich, D. J. Lindsay, J. C. Drazen, A. Vereshchaka, U. Piatkowski, T. Morato, K. Błachowiak-Samołyk, B. H. Robison, K. M. Gjerde, A. Pierrot-Bults, P. Bernal, G. Reygondeau, M. Heino, A global biogeographic classification of the mesopelagic zone. *Deep Sea Res. Part 1 Oceanogr. Res. Pap.* **126**, 85–102 (2017).

29. M. R. Stukel, T. B. Kelly, M. R. Landry, K. E. Selph, R. Swalethorp, Sinking carbon, nitrogen, and pigment flux within and beneath the euphotic zone in the oligotrophic, open-ocean Gulf of Mexico. *J. Plankton Res.* **44**, 711–727 (2022).

30. W.-J. Cai, X. Hu, W.-J. Huang, M. C. Murrell, J. C. Lehrter, S. E. Lohrenz, W.-C. Chou, W. Zhai, J. T. Hollibaugh, Y. Wang, P. Zhao, X. Guo, K. Gundersen, M. Dai, G.-C. Gong, Acidification of subsurface coastal waters enhanced by eutrophication. *Nat. Geosci.* **4**, 766–770 (2011).

31. R. Wanninkhof, L. Barbero, R. Byrne, W.-J. Cai, W.-J. Huang, J.-Z. Zhang, M. Baringer, C. Langdon, Ocean acidification along the Gulf Coast and East Coast of the USA. *Cont. Shelf Res.* **98**, 54–71 (2015).

32. R. H. Weisberg, L. Zheng, Y. Liu, West Florida shelf upwelling: Origins and pathways. *J. Geophys. Res. C: Oceans* **121**, 5672–5681 (2016).

33. E. R. Hall, K. K. Yates, K. A. Hubbard, M. J. Garrett, J. D. Frankle, Nutrient and carbonate chemistry patterns associated with *Karenia brevis* blooms in three West Florida Shelf estuaries 2020-2023. *Frontiers in Marine Science* **11** (2024).

34. M. J. Ulloa, P. Álvarez-Torres, K. P. Horak-Romo, R. Ortega-Izaguirre, Harmful algal blooms and eutrophication along the mexican coast of the Gulf of Mexico large marine ecosystem. *Environmental Development* **22**, 120–128 (2017).

35. C. A. Heil, A. L. Muni-Morgan, Florida's Harmful Algal Bloom (HAB) Problem: Escalating Risks to Human, Environmental and Economic Health With Climate Change. *Frontiers in Ecology and Evolution* **9** (2021).

36. P. M. Brannock, A. C. Ortmann, A. G. Moss, K. M. Halanych, Metabarcoding reveals environmental factors influencing spatio-temporal variation in pelagic micro-eukaryotes. *Mol. Ecol.* **25**, 3593–3604 (2016).

37. C. G. Easson, J. V. Lopez, Depth-Dependent Environmental Drivers of Microbial Plankton Community Structure in the Northern Gulf of Mexico. *Front. Microbiol.* **9**, 3175 (2018).

38. K. Sidón-Ceseña, M. A. Martínez-Mercado, J. Chong-Robles, Y. Ortega-Saad, V. F. Camacho-Ibar, L. Linacre, A. Lago-Lestón, Response of microbial eukaryote community to the oligotrophic waters of the Gulf of Mexico: a plausible scenario for warm and stratified oceans, *bioRxiv* (2023)

39. M. W. Henson, J. C. Thrash, Microbial ecology of northern Gulf of Mexico estuarine waters. *mSystems*, e0131823 (2024).

40. B. B. Tolar, G. M. King, J. T. Hollibaugh, An analysis of thaumarchaeota populations from the northern Gulf of Mexico. *Front. Microbiol.* **4**, 72 (2013).

41. Thrash J. Cameron, Seitz Kiley W., Baker Brett J., Temperton Ben, Gillies Lauren E., Rabalais Nancy N., Henrissat Bernard, Mason Olivia U., Metabolic Roles of Uncultivated Bacterioplankton Lineages in the Northern Gulf of Mexico "Dead Zone." *MBio* **8**, 10.1128/mbio.01017–17 (2017).

42. C. de Vargas, S. Audic, N. Henry, J. Decelle, F. Mahe, R. Logares, E. Lara, C. Berney, N. L. Bescot, I. Probert, M. Carmichael, J. Poulain, S. Romac, S. Colin, J.-M. Aury, L. Bittner, S. Chaffron, M. Dunthorn, S. Engelen, O. Flegontova, L. Guidi, A. Horak, O. Jaillon, G. Lima-Mendez, J. Luke, S. Malviya, R. Morard, M. Mulot, E. Scalco, R. Siano, F. Vincent, A. Zingone, C. Dimier, M. Picheral, S. Searson, S. Kandels-Lewis, T. O. Coordinators, S. G. Acinas, P. Bork, C. Bowler, G. Gorsky, N. Grimsley, P. Hingamp, D. Iudicone, F. Not, H. Ogata, S. Pesant, J. Raes, M. E. Sieracki, S. Speich, L. Stemmann, S. Sunagawa, J. Weissenbach, P. Wincker, E. Karsenti, E. Boss, M. Follows, L. Karp-Boss, U. Krzic, E. G. Reynaud, C. Sardet, M. B. Sullivan, D. Velayoudon, Eukaryotic plankton diversity in the sunlit ocean. *Science* **348**, 1261605–1261605 (2015).

43. S. Sunagawa, L. P. Coelho, S. Chaffron, J. R. Kultima, K. Labadie, G. Salazar, B. Djahanschiri, G. Zeller, D. R. Mende, A. Alberti, F. M. Cornejo-Castillo, P. I. Costea, C. Cruaud, F. d'Ovidio, S. Engelen, I. Ferrera, J. M. Gasol, L. Guidi, F. Hildebrand, F. Kokoszka, C. Lepoivre, G. Lima-Mendez, J. Poulain, B. T. Poulos, M. Royo-Llonch, H. Sarmento, S. Vieira-Silva, C. Dimier, M. Picheral, S. Searson, S. Kandels-Lewis, T. O. Coordinators, C. Bowler, C. de Vargas, G. Gorsky, N. Grimsley, P. Hingamp, D. Iudicone, O. Jaillon, F. Not, H. Ogata, S. Pesant, S. Speich, L. Stemmann, M. B. Sullivan, J. Weissenbach, P. Wincker, E. Karsenti, J. Raes, S. G. Acinas, P. Bork, Structure and function of the global ocean microbiome. *Science* **348**, 1261359– 1261359

(05 2015).

44. A. Djurhuus, P. H. Boersch-Supan, S.-O. Mikalsen, A. D. Rogers, Microbe biogeography tracks water masses in a dynamic oceanic frontal system. *R Soc Open Sci* **4**, 170033 (2017).

45. J. K. Pearman, B. Jones, M. Qashqari, S. Carvalho, Eukaryotic diversity patterns in the Red Sea: from the surface to the deep. *Frontiers in Marine Science* **10** (2024).

46. E. A. Walsh, J. B. Kirkpatrick, S. D. Rutherford, D. C. Smith, M. Sogin, S. D'Hondt, Bacterial diversity and community composition from seasurface to subseafloor. *ISME J.* **10**, 979–989 (2016).

47. T. Pommier, P. R. Neal, J. M. Gasol, M. Coll, S. G. Acinas, C. Pedrós-Alió, Spatial patterns of bacterial richness and evenness in the NW Mediterranean Sea explored by pyrosequencing of the 16S rRNA. *Aquat. Microb. Ecol.* **61**, 221–233 (2010).

48. Y.-C. Yeh, J. A. Fuhrman, Contrasting diversity patterns of prokaryotes and protists over time and depth at the San-Pedro Ocean Time series. *ISME Commun* **2**, 36 (2022).

49. N. V. Patin, Z. A. Dietrich, A. Stancil, M. Quinan, J. S. Beckler, E. R. Hall, J. Culter, C. G. Smith, M. Taillefert, F. J. Stewart, Gulf of Mexico blue hole harbors high levels of novel microbial lineages. *ISME J.* **15**, 2206–2232 (2021).

50. A. E. Santoro, C. Buchwald, M. R. McIlvin, K. L. Casciotti, Isotopic signature of N(2)O produced by marine ammonia-oxidizing archaea. *Science* **333**, 1282–1285 (2011).

51. Z. I. Johnson, E. R. Zinser, A. Coe, N. P. McNulty, E. M. S. Woodward, S. W. Chisholm, Niche partitioning among *Prochlorococcus* ecotypes along ocean-scale environmental gradients. *Science* **311**, 1737– 1740 (03 2006).

52. D. Tsementzi, J. Wu, S. Deutsch, S. Nath, L. M. Rodriguez-R, A. S. Burns, P. Ranjan, N. Sarode, R. R. Malmstrom, C. C. Padilla, B. K. Stone, L. A. Bristow, M. Larsen, J. B. Glass, B. Thamdrup, T. Woyke, K. T. Konstantinidis, F. J. Stewart, SAR11 bacteria linked to ocean anoxia and nitrogen loss. *Nature* **536**, 179– 183 (08 2016).

53. K. E. Selph, R. Swalethorp, M. R. Stukel, T. B. Kelly, A. N. Knapp, K. Fleming, T. Hernandez, M. R. Landry, Phytoplankton community composition and biomass in the oligotrophic Gulf of Mexico. *J. Plankton Res.* **44**, 618–637 (2022).

54. R. Massana, J. del Campo, M. E. Sieracki, S. Audic, R. Logares, Exploring the uncultured microeukaryote majority in the oceans: reevaluation of ribogroups within stramenopiles. *ISME J.* **8**, 854–866 (2014).

55. T. Biard, Diversity and ecology of Radiolaria in modern oceans. *Environ. Microbiol.* **24**, 2179–2200 (2022).

56. L. Guillou, M. Viprey, A. Chambouvet, R. M. Welsh, A. R. Kirkham, R. Massana, D. J. Scanlan, A. Z. Worden, Widespread occurrence and genetic diversity of marine

parasitoids belonging to Syndiniales (Alveolata). *Environ. Microbiol.* **10**, 3349–3365 (2008).

57. T. Cordier, I. B. Angeles, N. Henry, F. Lejzerowicz, C. Berney, R. Morard, A. Brandt, M.-A. Cambon-Bonavita, L. Guidi, F. Lombard, P. M. Arbizu, R. Massana, C. Orejas, J. Poulain, C. R. Smith, P. Wincker, S. Arnaud-Haond, A. J. Gooday, C. de Vargas, J. Pawlowski, Patterns of eukaryotic diversity from the surface to the deep-ocean sediment. *Science Advances* **8**, eabj9309 (2022).

58. C. A. Durkin, I. Cetinić, M. Estapa, Z. Ljubešić, M. Mucko, A. Neeley, M. Omand, Tracing the path of carbon export in the ocean through DNA sequencing of individual sinking particles. *ISME J.*, 1–11 (2022).

59. O. Flegontova, P. Flegontov, S. Malviya, S. Audic, P. Wincker, C. de Vargas, C. Bowler, J. Lukeš, A. Horák, Extreme Diversity of Diplonemid Eukaryotes in the Ocean. *Curr. Biol.* **26**, 3060–3065 (2016).

60. J. Saltzman, E. R. White, Determining the role of environmental covariates on planktivorous elasmobranch population trends within an isolated marine protected area. *Mar. Ecol. Prog. Ser*. **722**, 107–123 (2023).

61. E. Bravo-Ormaza, R. Arauz, S. Bessudo, A. Hearn, A. P. Klimley, F. Ladino-Archila, J. López-Macías, T. Steiner, C. Peñaherrera-Palma, Scalloped hammerhead shark *Sphyrna lewini* relative abundance comparison in three offshore marine protected areas of the Eastern Tropical Pacific. *Environ. Biol. Fishes*, doi: 10.1007/s10641-023-01454-6 (2023).

62. A. F. Zuur, E. N. Ieno, C. S. Elphick, A protocol for data exploration to avoid common statistical problems. *Methods Ecol. Evol.* **1**, 3–14 (2010).

63. F. E. Muller-Karger, J. P. Smith, S. Werner, R. Chen, M. Roffer, Y. Liu, B. Muhling, D. Lindo-Atichati, J. Lamkin, S. Cerdeira-Estrada, D. B. Enfield, Natural variability of surface oceanographic conditions in the offshore Gulf of Mexico. *Prog. Oceanogr.* **134**, 54–76 (2015).

64. N. Yingling, T. B. Kelly, T. A. Shropshire, M. R. Landry, K. E. Selph, A. N. Knapp, S. A. Kranz, M. R. Stukel, Taxon-specific phytoplankton growth, nutrient utilization and light limitation in the oligotrophic Gulf of Mexico. *J. Plankton Res.* **44**, 656–676 (2022).

65. X. A. G. Morán, L. Alonso-Sáez, E. Nogueira, H. W. Ducklow, N. González, Á. López-Urrutia, L. Díaz-Pérez, A. Calvo-Díaz, N. Arandia-Gorostidi, T. M. Huete-Stauffer, More, smaller bacteria in response to ocean's warming? *Proc. Biol. Sci.* **282** (2015).

66. N. Arandia-Gorostidi, P. K. Weber, L. Alonso-Sáez, X. A. G. Morán, X. Mayali, Elevated temperature increases carbon and nitrogen fluxes between phytoplankton and heterotrophic bacteria through physical attachment. *ISME J.* **11**, 641–650 (2017).

67. J. Taucher, J. Arístegui, L. T. Bach, W. Guan, M. F. Montero, A. Nauendorf, E. P. Achterberg, U. Riebesell, Response of Subtropical Phytoplankton Communities to Ocean

Acidification Under Oligotrophic Conditions and During Nutrient Fertilization. *Frontiers in Marine Science* **5** (2018).

68. M. W. Lomas, B. M. Hopkinson, J. L. Losh, D. E. Ryan, D. L. Shi, Y. Xu, F. M. M. Morel, Effect of ocean acidification on cyanobacteria in the subtropical North Atlantic. *Vol.* **66**, 211–222 (2012).

69. P. Flombaum, W.-L. Wang, F. W. Primeau, A. C. Martiny, Global picophytoplankton niche partitioning predicts overall positive response to ocean warming. *Nat. Geosci.* **13**, 116–120 (2020).

70. F.-X. Fu, M. E. Warner, Y. Zhang, Y. Feng, D. A. Hutchins, Effects of increased temperature and CO2 on photosynthesis, growth, and elemental ratios in marine *Synechococcus* and *Prochlorococcus* (cyanobacteria). *J. Phycol.* **43**, 485–496 (2007).

71. L. T. Bach, S. Alvarez-Fernandez, T. Hornick, A. Stuhr, U. Riebesell, Simulated ocean acidification reveals winners and losers in coastal phytoplankton. *PLoS One* **12**, e0188198 (2017).

72. A. Martiny, S. Kathuria, P. Berube, Widespread metabolic potential for nitrite and nitrate assimilation among *Prochlorococcus* ecotypes. *Proc. Natl. Acad. Sci. U. S. A.*, doi: 10.1073/pnas.0902532106 (06 2009).

73. J. H. Brown, J. F. Gillooly, A. P. Allen, V. M. Savage, G. B. West, Toward a metabolic theory of ecology. *Ecology* **85**, 1771–1789 (2004).

74. Y. Feng, F. Chai, M. L. Wells, Y. Liao, P. Li, T. Cai, T. Zhao, F. Fu, D. A. Hutchins, The Combined Effects of Increased pCO2 and Warming on a Coastal Phytoplankton Assemblage: From Species Composition to Sinking Rate. *Frontiers in Marine Science* **8** (2021).

75. H. G. Horn, N. Sander, A. Stuhr, M. Algueró-Muñiz, L. T. Bach, M. G. J. Löder, M. Boersma, U. Riebesell, N. Aberle, Low CO2 Sensitivity of Microzooplankton Communities in the Gullmar Fjord, Skagerrak: Evidence from a Long-Term Mesocosm Study. *PLoS One* **11**, e0165800 (2016).

76. D. K. Stoecker, P. J. Hansen, D. A. Caron, A. Mitra, Mixotrophy in the Marine Plankton. *Ann. Rev. Mar. Sci.* **9**, 311–335 (2017).

77. O. U. Mason, E. J. Canter, L. E. Gillies, T. K. Paisie, B. J. Roberts, Mississippi River Plume Enriches Microbial Diversity in the Northern Gulf of Mexico. *Front. Microbiol.* **7**, 1048 (2016).

78. F. A. Gomez, S.-K. Lee, F. J. Hernandez Jr, L. M. Chiaverano, F. E. Muller-Karger, Y. Liu, J. T. Lamkin, ENSO-induced co-variability of Salinity, Plankton Biomass and Coastal Currents in the Northern Gulf of Mexico. *Sci. Rep.* **9**, 178 (2019).

79. F. A. Gomez, R. Wanninkhof, L. Barbero, S.-K. Lee, F. J. Hernandez Jr, Seasonal patterns of surface inorganic carbon system variables in the Gulf of Mexico inferred from

a regional high-resolution ocean biogeochemical model. *Biogeosciences* **17**, 1685–1700 (2020).

80. A. K. Williams, A. S. McInnes, J. R. Rooker, A. Quigg, Changes in Microbial Plankton Assemblages Induced by Mesoscale Oceanographic Features in the Northern Gulf of Mexico. *PLoS One* **10**, e0138230 (2015).

81. S. Anglès, A. Jordi, D. W. Henrichs, L. Campbell, Influence of coastal upwelling and river discharge on the phytoplankton community composition in the northwestern Gulf of Mexico. *Prog. Oceanogr.* **173**, 26–36 (2019).

82. S. Wood, Generalized Additive Models: An Introduction with R (Chapman and Hall/CRC, 2017).

83. G. B. Gloor, J. M. Macklaim, V. Pawlowsky-Glahn, J. J. Egozcue, Microbiome Datasets Are Compositional: And This Is Not Optional. *Front. Microbiol.* **8**, 2224 (2017).

84. W. Gong, A. Marchetti, Estimation of 18S Gene Copy Number in Marine Eukaryotic Plankton Using a Next-Generation Sequencing Approach. *Frontiers in Marine Science* **6** (2019).

85. S. Collins, P. W. Boyd, M. A. Doblin, Evolution, Microbes, and Changing Ocean Conditions. *Ann. Rev. Mar. Sci.* **12**, 181–208 (2020).

86. F. Partensky, J. Blanchot, D. Vaulot, Differential distribution and ecology of *Prochlorococcus* and *Synechococcus* in oceanic waters: a review. *Bulletin de l'Institut océanographique. Monaco. n° spécial*, 457–475 (1999).

87. A. Buchan, G. R. LeCleir, C. A. Gulvik, J. M. González, Master recyclers: features and functions of bacteria associated with phytoplankton blooms. *Nat. Rev. Microbiol.* **12**, 686–698 (2014).

88. C. J. Gobler, Climate Change and Harmful Algal Blooms: Insights and perspective. *Harmful Algae* **91**, 101731 (2020).

89. R. M. Errera, S. Yvon-Lewis, J. D. Kessler, L. Campbell, Responses of the dinoflagellate *Karenia brevis* to climate change: pCO2 and sea surface temperatures. *Harmful Algae* **37**, 110–116 (2014).

90. B. A. Stauffer, H. A. Bowers, E. Buckley, T. W. Davis, T. H. Johengen, R. Kudela, M. A. McManus, H. Purcell, G. J. Smith, A. Vander Woude, M. N. Tamburri, Considerations in Harmful Algal Bloom Research and Monitoring: Perspectives From a Consensus-Building Workshop and Technology Testing. *Frontiers in Marine Science* **6** (2019).

91. E. S. Egleston, C. L. Sabine, F. M. M. Morel, Revelle revisited: Buffer factors that quantify the response of ocean chemistry to changes in DIC and alkalinity. *Global Biogeochem. Cycles* (2010).

92. A. Z. Worden, J. K. Nolan, B. Palenik, Assessing the dynamics and ecology of marine

picophytoplankton: The importance of the eukaryotic component. *Limnol. Oceanogr.* **49**, 168–179 (2004).

93. P. Ziveri, B. de Bernardi, K.-H. Baumann, H. M. Stoll, P. G. Mortyn, Sinking of coccolith carbonate and potential contribution to organic carbon ballasting in the deep ocean. *Deep Sea Res. Part 2 Top. Stud. Oceanogr.* **54**, 659–675 (2007).

94. C.-E. Schaum, B. Rost, S. Collins, Environmental stability affects phenotypic evolution in a globally distributed marine picoplankton. *ISME J.* **10**, 75–84 (2016).

95. K. T. Lohbeck, U. Riebesell, T. B. H. Reusch, Adaptive evolution of a key phytoplankton species to ocean acidification. *Nat. Geosci.* **5**, 346–351 (2012).

96. K.-H. Baumann, B. Boeckel, Spatial distribution of living coccolithophores in the southwestern Gulf of Mexico. *J. Micropalaeontol.* **32**, 123–133 (2013).

97. S. J. Giovannoni, SAR11 Bacteria: The Most Abundant Plankton in the Oceans. *Ann. Rev. Mar. Sci.* **9**, 231–255 (2017).

98. M. S. Rappé, S. A. Connon, K. L. Vergin, S. J. Giovannoni, Cultivation of the ubiquitous SAR11 marine bacterioplankton clade. *Nature* **418**, 630– 633 (08 2002).

99. N. R. Bates, Y. M. Astor, M. J. Church, K. Currie, J. E. Dore, M. González-Dávila, L. Lorenzoni, F. Muller-Karger, J. Olafsson, J. M. Santana-Casiano, A Time-Series View of Changing Surface Ocean Chemistry Due to Ocean Uptake of Anthropogenic CO_2 and Ocean Acidification. *Oceanography* **27**, 126–141 (2014).

100. S. Dutkiewicz, P. Cermeno, O. Jahn, M. J. Follows, A. E. Hickman, D. A. A. Taniguchi, B. A. Ward, Dimensions of marine phytoplankton diversity. *Biogeosciences* **17**, 609–634 (2020).

101. E. L. Cavan, S. A. Henson, P. W. Boyd, The Sensitivity of Subsurface Microbes to Ocean Warming Accentuates Future Declines in Particulate Carbon Export. *Frontiers in Ecology and Evolution* **6** (2019).

102. S. A. Henson, C. Laufkötter, S. Leung, S. L. C. Giering, H. I. Palevsky, E. L. Cavan, Uncertain response of ocean biological carbon export in a changing world. *Nat. Geosci.* **15**, 248–254 (2022).

103. C. Langdon, Determination of dissolved oxygen in seawater by Winkler titration using the amperometric technique. (2010).

104. J.-Z. Zhang, G. A. Berberian, Determination of dissolved silicate in estuarine and coastal waters by gas segmented continuous flow colorimetric analysis. *Methods for the determination of chemical substances in marine and estuarine environmental matrices*, 366–360 (1997).

105. K. M. Johnson, A. E. King, J. M. Sieburth, Coulometric TCO2 analyses for marine studies; an introduction. *Mar. Chem.* **16**, 61–82 (1985).

106. A. G. Dickson, C. L. Sabine, J. R. Christian,"Guide to best practices for ocean CO2 measurements" (Report, North Pacific Marine Science Organization, 2007).

107. R. Wanninkhof, K. Thoning, Measurement of fugacity of CO2 in surface water using continuous and discrete sampling methods. *Mar. Chem.* **44**, 189–204 (1993).

108. R. H. Byrne, L. R. Kump, K. J. Cantrell, The influence of temperature and pH on trace metal speciation in seawater. *Mar. Chem.* **25**, 163–181 (1988).

109. S. M. A. C. van Heuven, M. Hoppema, O. Huhn, H. A. Slagter, H. J. W. de Baar, Direct observation of increasing CO2 in the Weddell Gyre along the Prime Meridian during 1973–2008. *Deep Sea Res. Part 2 Top. Stud. Oceanogr.* **58**, 2613–2635 (2011).

110. S. R. Anderson, L. R. Thompson, Optimizing an enclosed bead beating extraction method for microbial and fish environmental DNA. *Environmental DNA*, doi: 10.1002/edn3.251 (2021).

111. A. E. Parada, D. M. Needham, J. A. Fuhrman, Every base matters: assessing small subunit rRNA primers for marine microbiomes with mock communities, time series and global field samples. *Environ. Microbiol.* **18**, 1403– 1414 (05 2016).

112. L. A. Amaral-Zettler, E. A. McCliment, H. W. Ducklow, S. M. Huse, A method for studying protistan diversity using massively parallel sequencing of V9 hypervariable regions of small-subunit ribosomal RNA Genes. *PLoS One* **4**, e6372 (07 2009).

113. M. Martin, Cutadapt removes adapter sequences from high-throughput sequencing reads. *EMBnet.journal* **17**, 10–12 (2011).

114. L. R. Thompson, S. R. Anderson, P. A. Den Uyl, N. V. Patin, S. J. Lim, G. Sanderson, K. D. Goodwin, Tourmaline: A containerized workflow for rapid and iterable amplicon sequence analysis using QIIME 2 and Snakemake. *Gigascience* **11** (2022).

115. B. J. Callahan, P. J. Mcmurdie, S. P. Holmes, Exact sequence variants should replace operational taxonomic units in marker-gene data analysis. *ISME J.* **11**, 2639–2643 (2016).

116. E. Pruesse, C. Quast, K. Knittel, B. M. Fuchs, W. Ludwig, J. Peplies, F. O. Glöckner, SILVA: a comprehensive online resource for quality checked and aligned ribosomal RNA sequence data compatible with ARB. *Nucleic Acids Res.* **35**, 7188–7196 (2007).

117. L. Guillou, D. Bachar, S. Audic, D. Bass, C. Berney, L. Bittner, C. Boutte, G. Burgaud, C. De Vargas, J. Decelle, J. Del Campo, J. R. Dolan, M. Dunthorn, B. Edvardsen, M. Holzmann, W. H. C. F. Kooistra, E. Lara, N. Le Bescot, R. Logares, F. Mahé, R. Massana, M. Montresor, R. Morard, F. Not, J. Pawlowski, I. Probert, A. L. Sauvadet, R. Siano, T. Stoeck, D. Vaulot, P. Zimmermann, R. Christen, The Protist Ribosomal Reference database (PR2): A catalog of unicellular eukaryote Small Sub-Unit rRNA sequences with curated taxonomy. *Nucleic Acids Res.* **41** (2013).

118. N. A. Bokulich, B. D. Kaehler, J. R. Rideout, M. Dillon, E. Bolyen, R. Knight, G. A.

Huttley, J. Gregory Caporaso, Optimizing taxonomic classification of marker-gene amplicon sequences with QIIME 2's q2-feature-classifier plugin. *Microbiome* **6**, 90 (2018).

119. P. J. McMurdie, S. Holmes, Phyloseq: An R Package for Reproducible Interactive Analysis and Graphics of Microbiome Census Data. *PLoS One* **8** (2013).

120. G. S. Kandlikar, Z. J. Gold, M. C. Cowen, R. S. Meyer, A. C. Freise, N. J. B. Kraft, J. Moberg-Parker, J. Sprague, D. J. Kushner, E. E. Curd, ranacapa: An R package and Shiny web app to explore environmental DNA data with exploratory statistics and interactive visualizations. *F1000Res.* **7**, 1734 (2018).

121. A. Mitra, D. A. Caron, E. Faure, K. J. Flynn, S. G. Leles, P. J. Hansen, G. B. McManus, F. Not, H. do Rosario Gomes, L. F. Santoferrara, D. K. Stoecker, U. Tillmann, The Mixoplankton Database (MDB): Diversity of photo-phago-trophic plankton in form, function, and distribution across the global ocean. *J. Eukaryot. Microbiol.* **70**, e12972 (2023).

122. J. Oksanen, F. G. Blanchet, M. Friendly, R. Kindt, P. Legendre, D. McGlinn, P. R. Minchin, R. B. O'Hara, G. L. Simpson, P. Solymos, M. H. H. Stevens, E. Szoecs, H. Wagne, Vegan: Community ecology package. R package version 2.6-6.1 (2024).

123. A. Kassambara, Practical Guide to Cluster Analysis in R: Unsupervised Machine Learning Vol. 1 (Sthda, 2017).

124. L. Kaufman, P. J. Rousseeuw, Finding Groups in Data: An Introduction to Cluster Analysis (John Wiley & Sons, 2009).

125. H. Wickham, M. Averick, J. Bryan, W. Chang, L. McGowan, R. François, G. Grolemund, A. Hayes, L. Henry, J. Hester, M. Kuhn, T. Pedersen, E. Miller, S. Bache, K. Müller, J. Ooms, D. Robinson, D. Seidel, V. Spinu, K. Takahashi, D. Vaughan, C. Wilke, K. Woo, H. Yutani, Welcome to the tidyverse. *J. Open Source Softw.* **4**, 1686 (2019).

126. C. Liu, Y. Cui, X. Li, M. Yao, microeco: an R package for data mining in microbial community ecology. *FEMS Microbiol. Ecol.* **97**, fiaa255 (2021).

127. B. Bederson, B. Shneiderman, M. Wattenberg, Ordered and quantum treemaps: Making effective use of 2D space to display hierarchies. *ACM Trans. Graph.* **21**, 833–854 (2002).

128. M. De Cáceres, P. Legendre, M. Moretti, Improving indicator species analysis by combining groups of sites. *Oikos* **119**, 1674–1684 (2010).

129. G. James, D. Witten, T. Hastie, R. Tibshirani, An Introduction to Statistical Learning (Springer, 2013), vol. 112.

130. B. Ripley, B. Venables, D. M. Bates, K. Hornik, A. Gebhardt, D. Firth, M. B. Ripley, Package "mass." *Cran r* **538**, 113–120 (2013).

131. D. Lüdecke, M. Ben-Shachar, I. Patil, P. Waggoner, D. Makowski, Performance: An R

package for assessment, comparison and testing of statistical models. *J. Open Source Softw.* **6**, 3139 (2021).

132. J. P. Lander, coefplot: Plots coefficients from fitted models. R package version 1.2.8 (2022).

133. D. Lüdecke, sjPlot: Data visualization for statistics in social science. R package version 2.8.16 (2024).

134. R. Schlitzer, Ocean Data View. https://odv.awi.de (2023).

Acknowledgements

We thank the captain and crew of the NOAA Ship *Ronald H. Brown* for logistical support for sample collection in the Gulf. We acknowledge the efforts of many scientists at NOAA and partnering institutions for collecting and processing oceanographic data on GOMECC-4. We thank Easton White and Elizabeth Harvey for their helpful conversations, and Sean McAllister for carefully reviewing the manuscript. We acknowledge the genomics services performed in the RTSF Genomics Core at Michigan State University.

Funding: This work was funded in part through the NOAA Ocean Acidification Program (OAP) ROR #02bfn4816 under project numbers 21392 (Thompson) and 20708 (Barbero) and by awards NA16OAR4320199 and NA21OAR4320190 to the Northern Gulf Institute from NOAA's Office of Oceanic and Atmospheric Research, U.S. Department of Commerce. This research was carried out in part under the auspices of the Cooperative Institute for Marine and Atmospheric Studies (CIMAS) and NOAA, cooperative agreement NA20OAR4320472. This work was also supported by NSF award OCE-2019589 for the Center for Chemical Currencies of a Microbial Planet (C-CoMP). This is C-CoMP publication #046.

Author contributions: LRT, SRA, LB, and CRK conceived the study. SRA collected DNA samples. LB led collection of carbonate chemistry parameters. SRA and LRT processed DNA samples. SRA performed bioinformatics and data analysis. LRT, KS, and FAG contributed to improve data analysis. BAS and AS provided guidance on taxonomy and functional assignments. SRA and LRT led the writing of the manuscript. All authors contributed to revising the manuscript and approved the final version.

Competing interests: Authors declare that they have no competing interests.

Data and materials availability: Code and associated files needed to reproduce results and figures for this study are available on GitHub (https://github.com/aomlomics/gomecc) and have been archived on Zenodo (https://zenodo.org/records/13102580). All 18S and 16S sequence data generated from this study have been published at the National Center for Biotechnology Information (NCBI)'s Sequence Read Archive and BioSample database and are available with BioProject accession number PRJNA887898. Species count data generated from this study have been published on the Ocean Biodiversity Information System (OBIS) and the Global Biodiversity Information Facility (GBIF) at https://doi.org/10.15468/sm6fpz. Biological data has also been submitted to the National Centers for Environmental Information (NCEI) at https://www.ncei.noaa.gov/archive/accession/0250940/data/0-data/noaa-aoml-gomecc. Environmental measurements from the Niskin bottles and CTD profiles are also available at NCEI at https://doi.org/10.25921/4twf-pp50 and https://doi.org/10.25921/04h7-gv36, respectively. A cruise report detailing all the sampling and analyzing procedures during GOMECC-4 is available at https://doi.org/10.25923/rwx5-s713.

1266 **Figures and Tables**

1267

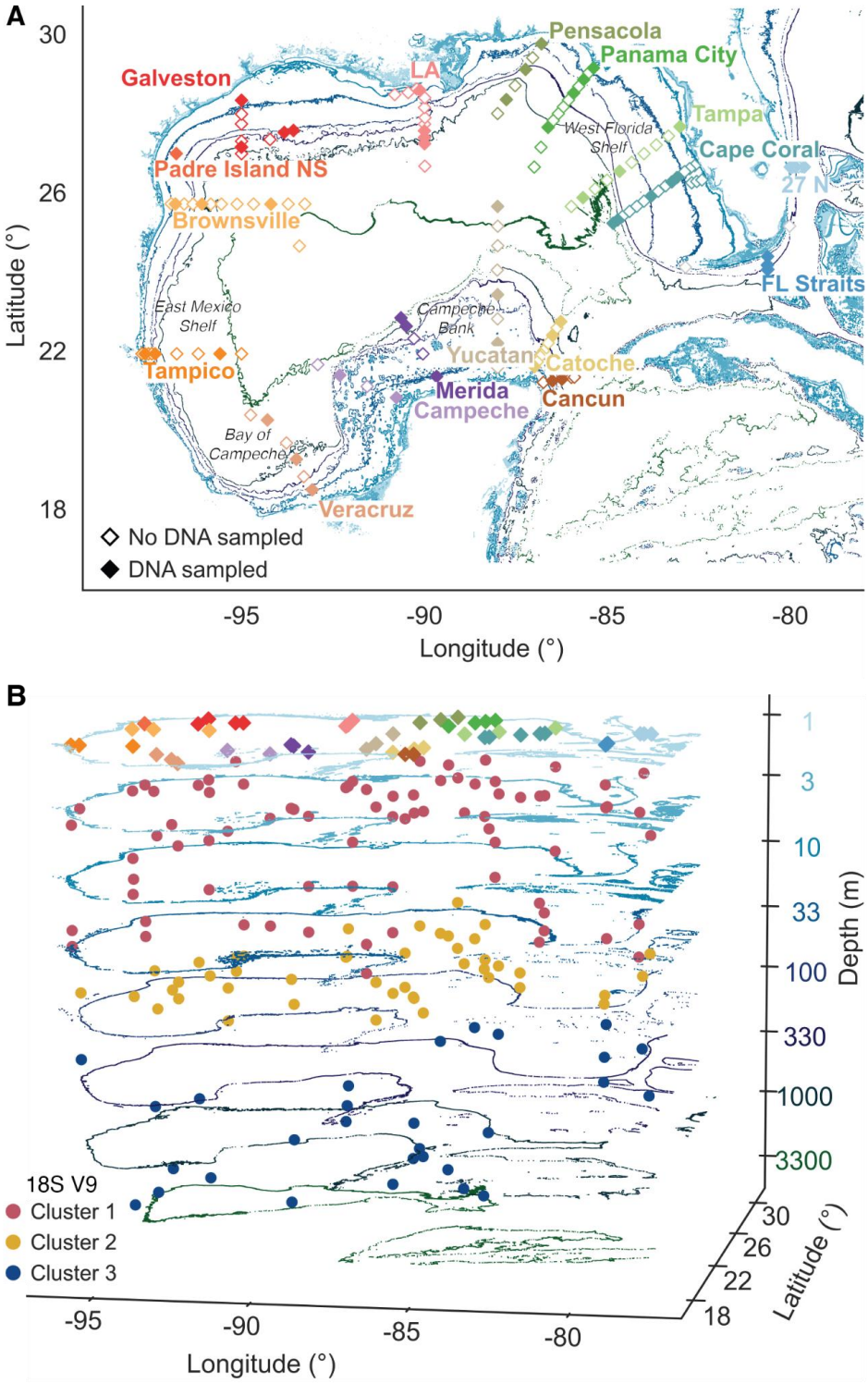

1268

Figure 1: Vertical and horizontal DNA sampling across the GOM. (A) Map of all sites sampled on GOMECC-4. Sites are colored by transect and indicate instances where DNA was (filled) or was not (empty) sampled. Samples at all sites were collected in triplicate. Environmental metadata was collected from all stations. Contour lines indicate depth in the GOM and correspond to the right y-axis in panel **B**. Transects are also labeled to match the color of stations along a given transect. Samples were collected counterclockwise in the Gulf starting at the 27°N line. **(B)** Map displaying depth-related position (log scale) of samples across the GOM. Stations are colored by transect at the surface, matching transect colors in panel **A**. Samples with depth are colored by their clusters (Clusters 1–3) that were determined via hierarchical clustering of Aitchison distances and largely reflected depth in the water column. Cluster 1 generally corresponded to shelf waters at all depths and in the open GOM at the surface (photic zone; n = 235), Cluster 2 represented sites in the DCM in the open GOM (DCM; n = 137), and Cluster 3 was confined to open ocean sites in deep waters (aphotic zone; n = 89). Clustering was similar between 18S (shown) and 16S samples (fig. S16).

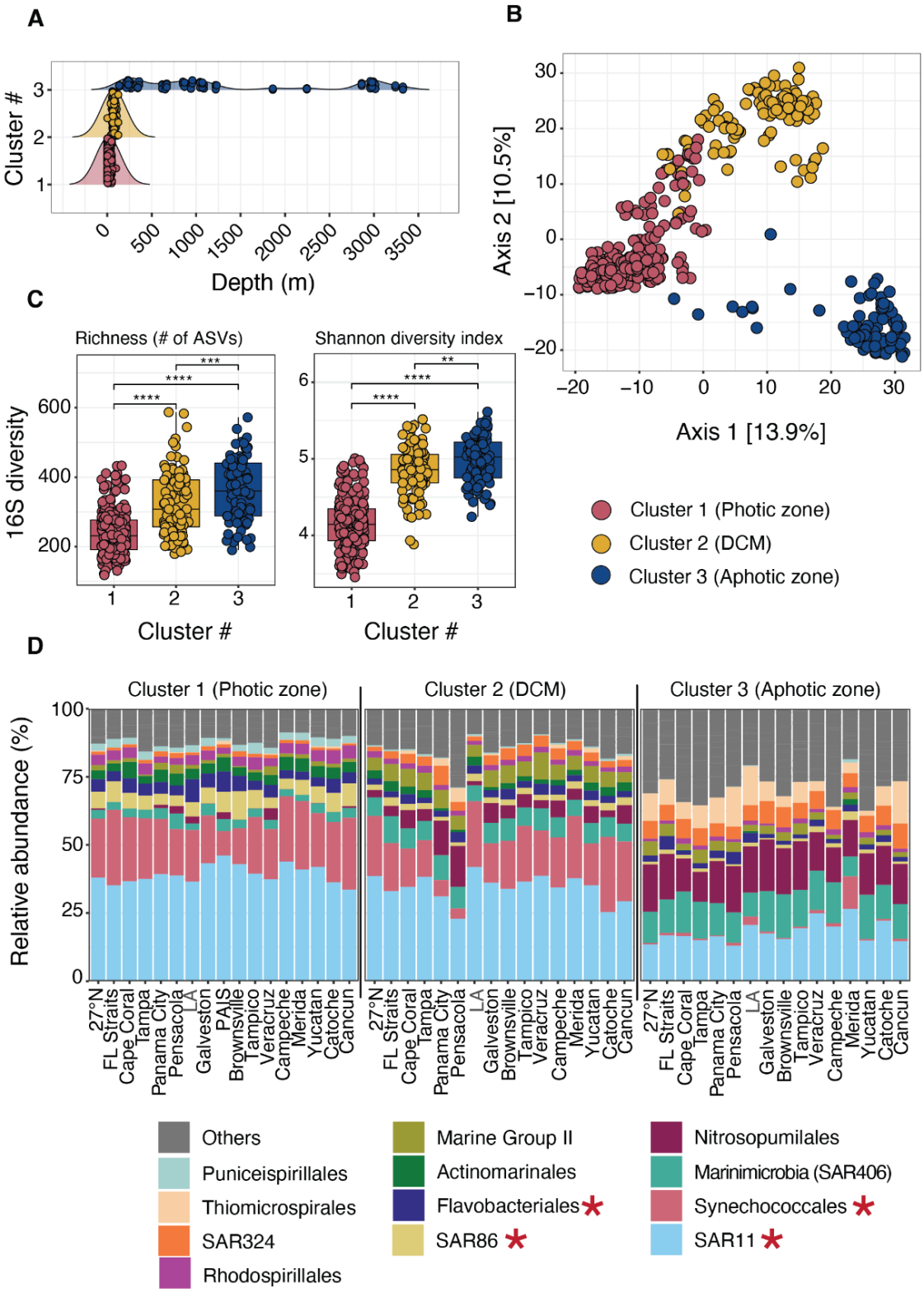
A
Cluster #
Depth (m)
B
Axis 2 [10.5%]
Axis 1 [13.9%]
Cluster 1 (Photic zone)
Cluster 2 (DCM)
Cluster 3 (Aphotic zone)
C
Richness (# of ASVs)
Shannon diversity index
16S diversity
Cluster #
D
Relative abundance (%)
Cluster 1 (Photic zone)
Cluster 2 (DCM)
Cluster 3 (Aphotic zone)
27°N
FL Straits
Cape Coral
Tampa
Panama City
Pensacola
LA
Galveston
PAIS
Brownsville
Tampico
Veracruz
Campeche
Merida
Yucatan
Catoche
Cancun
Others
Puniceispirillales
Thiomicrospirales
SAR324
Rhodospirillales
Marine Group II
Actinomarinales
Flavobacteriales
SAR86
Nitrosopumilales
Marinimicrobia (SAR406)
Synechococcales
SAR11

1284

Figure 2: Bacterial and archaeal community dynamics in the GOM from 16S metabarcoding. (A) Ridgeline plots showing the depth distribution of samples within each cluster (Clusters 1–3). Clusters were determined via hierarchical clustering of Aitchison distances: Cluster 1 (photic zone), Cluster 2 (DCM), and Cluster 3 (aphotic zone). **(B)** Principal coordinates analysis of Aitchison distances, with samples colored by their respective clusters. **(C)** Mean observed richness (# of ASVs) and Shannon diversity index for Clusters 1–3, with points representing individual samples. Significant differences between clusters were determined with Wilcoxon tests (** $P < 0.01$, *** $P < 0.001$, **** $P < 0.0001$). **(D)** Stacked bar plots of mean relative abundance (%) at the order level in each sampling transect and faceted by cluster. Transects are ordered on the x-axis based on the order of sampling (counterclockwise) on GOMECC-4, except for FL straits and Cape Coral that were sampled last but grouped spatially with other FL lines. Bar plots display the top 12 most relatively abundant groups over all samples ("others" in gray). Taxonomy was assigned via the SILVA database. Generalized linear models focused on the top four most relatively abundant groups in Cluster 1 (red asterisks). Models for Synechococcales were constructed at the genus level to discriminate between *Prochlorococcus* and *Synechococcus*. LA = Louisiana and PAIS = Padre Island National Seashore. Transects have the same labels in all subsequent plots.

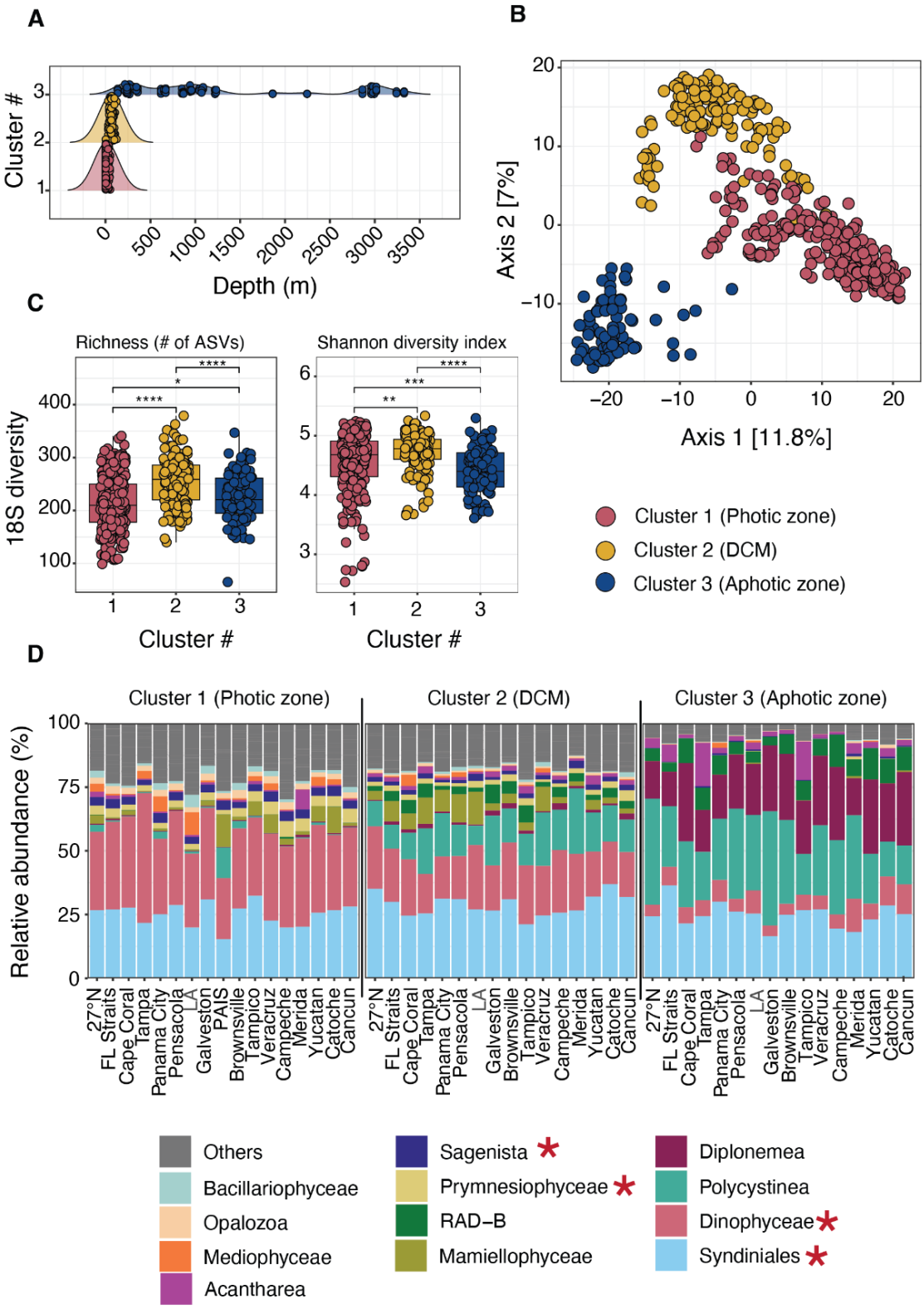
A
Cluster #
Depth (m)
B
Axis 2 [7%]
Axis 1 [11.8%]
Cluster 1 (Photic zone)
Cluster 2 (DCM)
Cluster 3 (Aphotic zone)
C
Richness (# of ASVs)
Shannon diversity index
18S diversity
Cluster #
D
Relative abundance (%)
27°N
FL Straits
Cape Coral
Tampa
Panama City
Pensacola
LA
Galveston
PAIS
Brownsville
Tampico
Veracruz
Campeche
Merida
Yucatan
Catoche
Cancun
Others
Bacillariophyceae
Opalozoa
Mediophyceae
Acantharea
Sagenista
Prymnesiophyceae
RAD–B
Mamiellophyceae
Diplonemea
Polycystinea
Dinophyceae
Syndiniales

1303

Figure 3: Protist community dynamics in the GOM from 18S metabarcoding. (A) Ridgeline plots showing the depth distribution of samples within each cluster (Clusters 1–3). Clusters reflected depth along the shelf and open GOM and closely resembled clustering of 16S samples**.** **(B)** Principal coordinates analysis of Aitchison distances, with 18S samples colored by cluster. **(C)** Mean observed richness (# of ASVs) and Shannon diversity index for Clusters 1–3, with points representing individual samples. Significant differences between clusters were determined with Wilcoxon tests (* $P < 0.05$, ** $P < 0.01$, *** $P < 0.001$, **** $P < 0.0001$). **(D)** Stacked bar plots of mean relative abundance (%) at the class level in each sampling transect and faceted by cluster. Transects are ordered the same as in Fig. 2. Bar plots display the top 12 most relatively abundant groups over all samples ("others" in gray). Protist taxonomy was assigned via the PR2 database. Generalized linear models focused on the top four most relatively abundant groups in Cluster 1 (red asterisks).

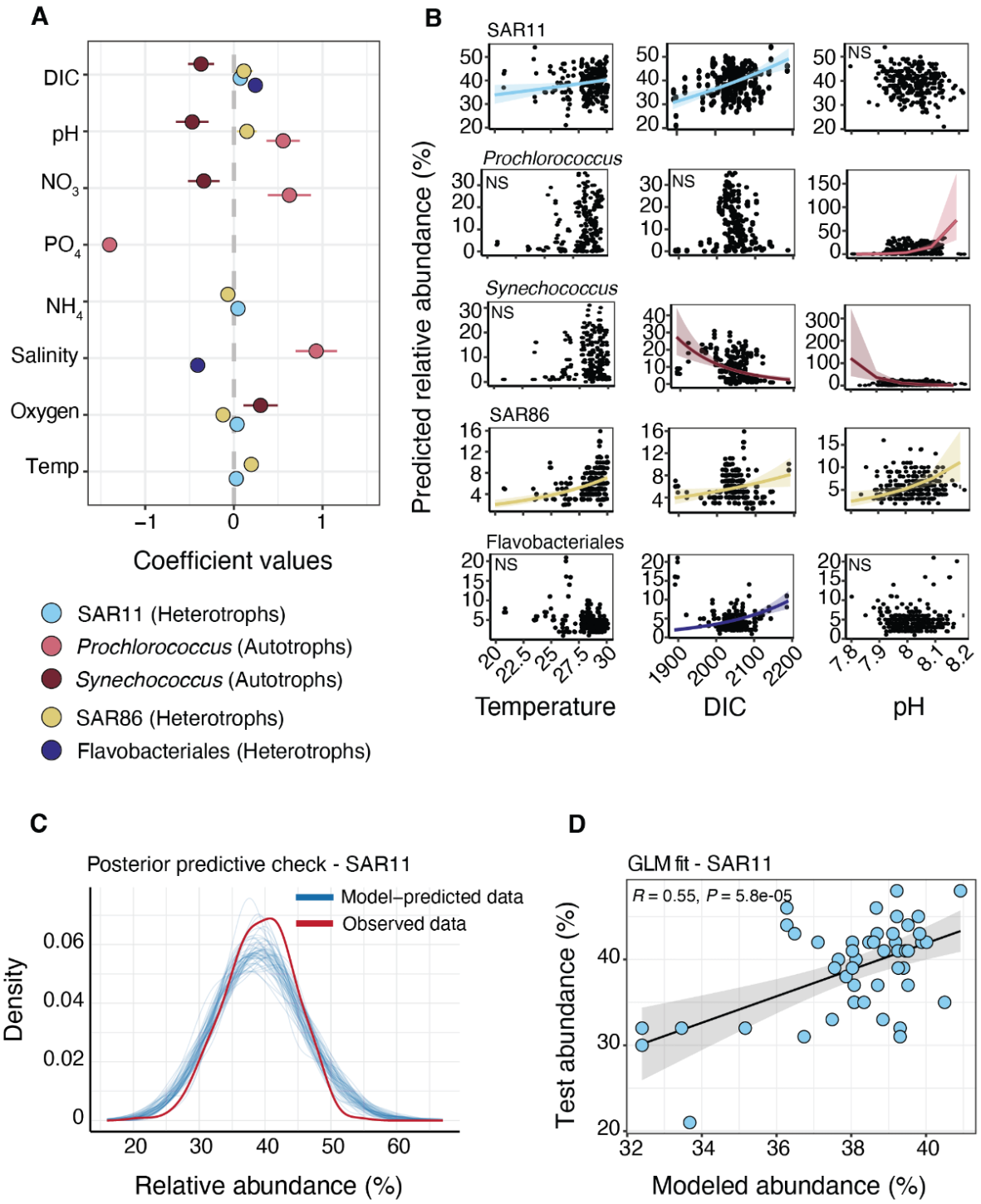
A
DIC
pH
NO3
PO4
NH4
Salinity
Oxygen
Temp
−1
0
1
Coefficient values
SAR11 (Heterotrophs)
Prochlorococcus (Autotrophs)
Synechococcus (Autotrophs)
SAR86 (Heterotrophs)
Flavobacteriales (Heterotrophs)
B
SAR11
Prochlorococcus
Synechococcus
SAR86
Flavobacteriales
NS
Predicted relative abundance (%)
Temperature
DIC
pH
C
Posterior predictive check - SAR11
Model−predicted data
Observed data
Density
Relative abundance (%)
D
GLM fit - SAR11
R = 0.55, P = 5.8e-05
Test abundance (%)
Modeled abundance (%)

1317

Figure 4: Generalized linear models of major 16S taxa reveal group-specific environmental drivers in the photic zone. (A) Scaled model coefficients (± 2 standard deviations) of predictor variables (environmental factors) that were significant to the final model (based on AIC values). Models were constructed with group-specific relative abundance as the response variable. The most relatively abundant 16S groups were modeled, which included heterotrophs and autotrophs. Models were generated at the order level, except for cyanobacteria (Synechococcales), where separate models were run for *Prochlorococcus* and *Synechococcus*. Only covariates that were statistically significant to a given model were plotted. **(B)** Predicted response estimates (relative abundance) and 95% confidence intervals (CIs) of major 16S groups to temperature, DIC, and in situ pH. NS = not significant. **(C)** An example of a posterior predictive plot, highlighting the fit of observed vs. model-predicted relative abundance for the final SAR11 model. The model-predicted data was simulated with 50 bootstraps and followed a similar trend as the observed data. **(D)** Pearson correlation (with 95% CI) between SAR11 test and modeled relative abundance to estimate model fit. Predicted abundance was derived from the final SAR11 model using a subset of the data (80%; 219 samples) and correlated to test data that was left out (20%; 48 samples). Model fit of other major 16S groups is shown in fig. S9.

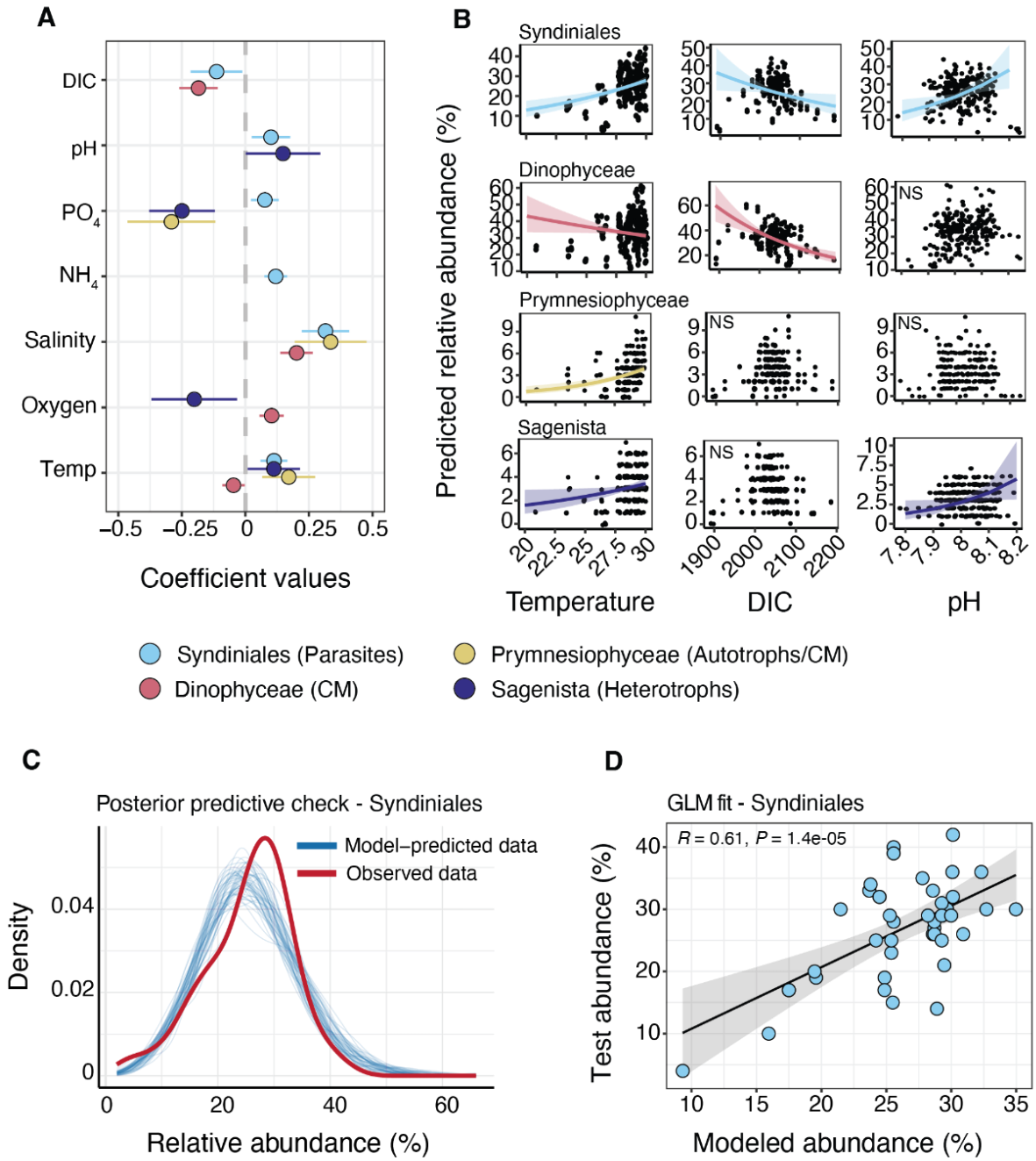
A
DIC
pH
PO4
NH4
Salinity
Oxygen
Temp
−0.5
−0.25
0
0.25
0.5
Coefficient values
B
Syndiniales
Dinophyceae
Prymnesiophyceae
Sagenista
Predicted relative abundance (%)
NS
Temperature
DIC
pH
Syndiniales (Parasites)
Dinophyceae (CM)
Prymnesiophyceae (Autotrophs/CM)
Sagenista (Heterotrophs)
C
Posterior predictive check - Syndiniales
Model−predicted data
Observed data
Density
Relative abundance (%)
D
GLM fit - Syndiniales
R = 0.61, P = 1.4e-05
Test abundance (%)
Modeled abundance (%)

1335

Figure 5: GLMs of major 18S taxa reveal group-specific drivers in the photic zone. (A) Scaled model coefficients (± 2 standard deviations) of predictor variables (environmental factors) that were significant to the final model (based on AIC values). Models were constructed with group-specific relative abundance as the response variable. The top four most relatively abundant 18S groups were modeled separately, spanning constitutive mixotrophs (CM), parasites, autotrophs, and heterotrophs. Covariates that were not statistically significant to a given model are not shown. **(B)** Predicted response estimates (relative abundance) and 95% confidence intervals (CIs) of major 18S groups to temperature, DIC, and pH. NS = not significant. **(C)** An example of a posterior predictive plot, highlighting the fit of observed vs. model-predicted relative abundance for the final Syndiniales model. The model-predicted data was simulated with 50 bootstraps and followed a similar trend as the observed data. **(D)** Pearson correlation (with 95% CI) between Syndiniales test and modeled relative abundance. Predicted abundance was derived from the final Syndiniales model using a subset of the data (80%; 187 samples) and correlated to test values that were left out (20%; 43 samples). Model fit of other major 18S groups is shown in fig. S10.

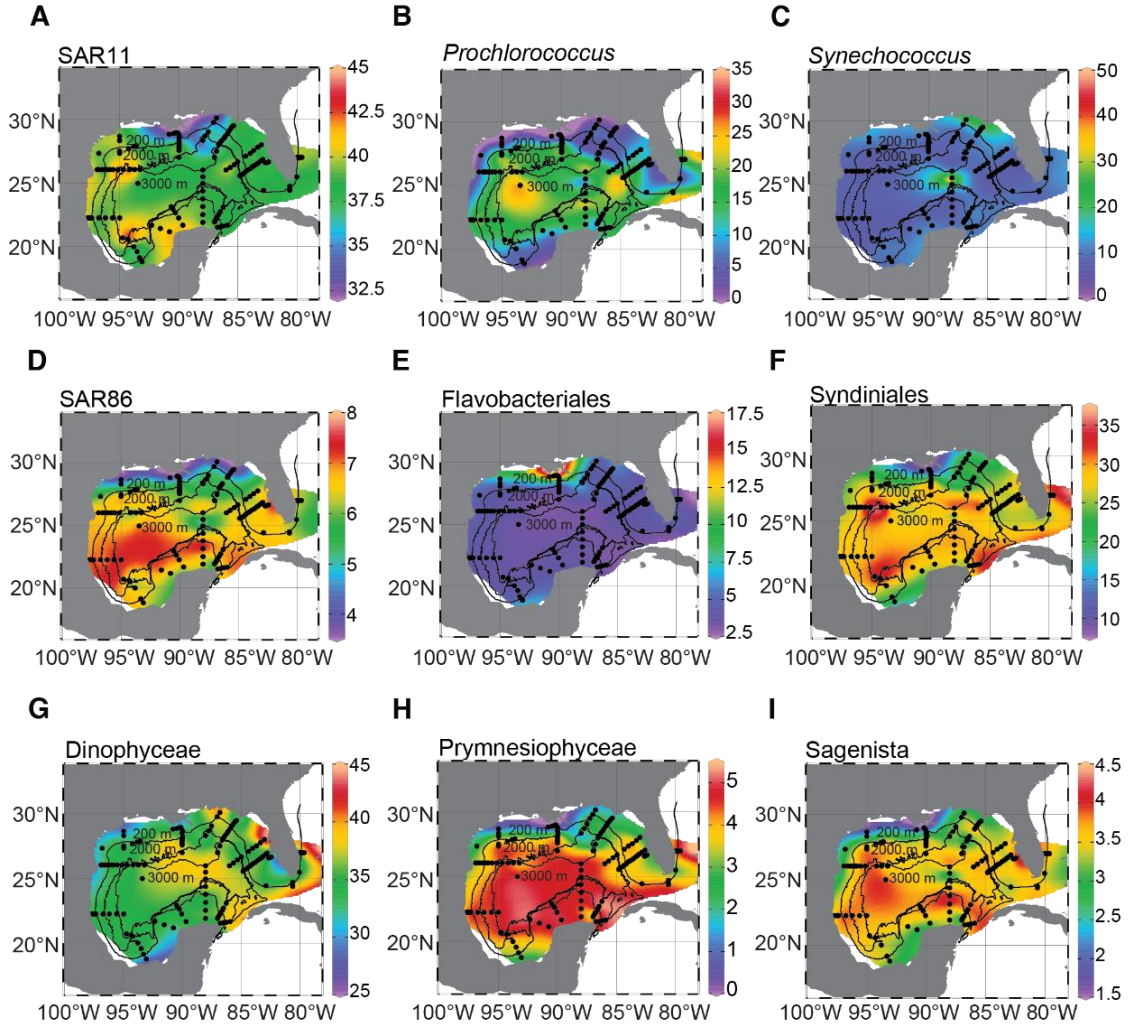

Figure 6: Expanding current microbial distributions in the GOM. Predicted relative abundance (%) of major 16S **(A–E)** and 18S groups **(F–I)** at 135 GOMECC-4 sites modeled with each respective GLM (from Table 2). Model results have been interpolated using DIVA interpolation in Ocean Data View. Isobaths are shown for 200 m, 2,000 m, and 3,000 m. Scales for predicted relative abundance vary by taxonomic group (on the right of each panel) but display low to high relative abundance.

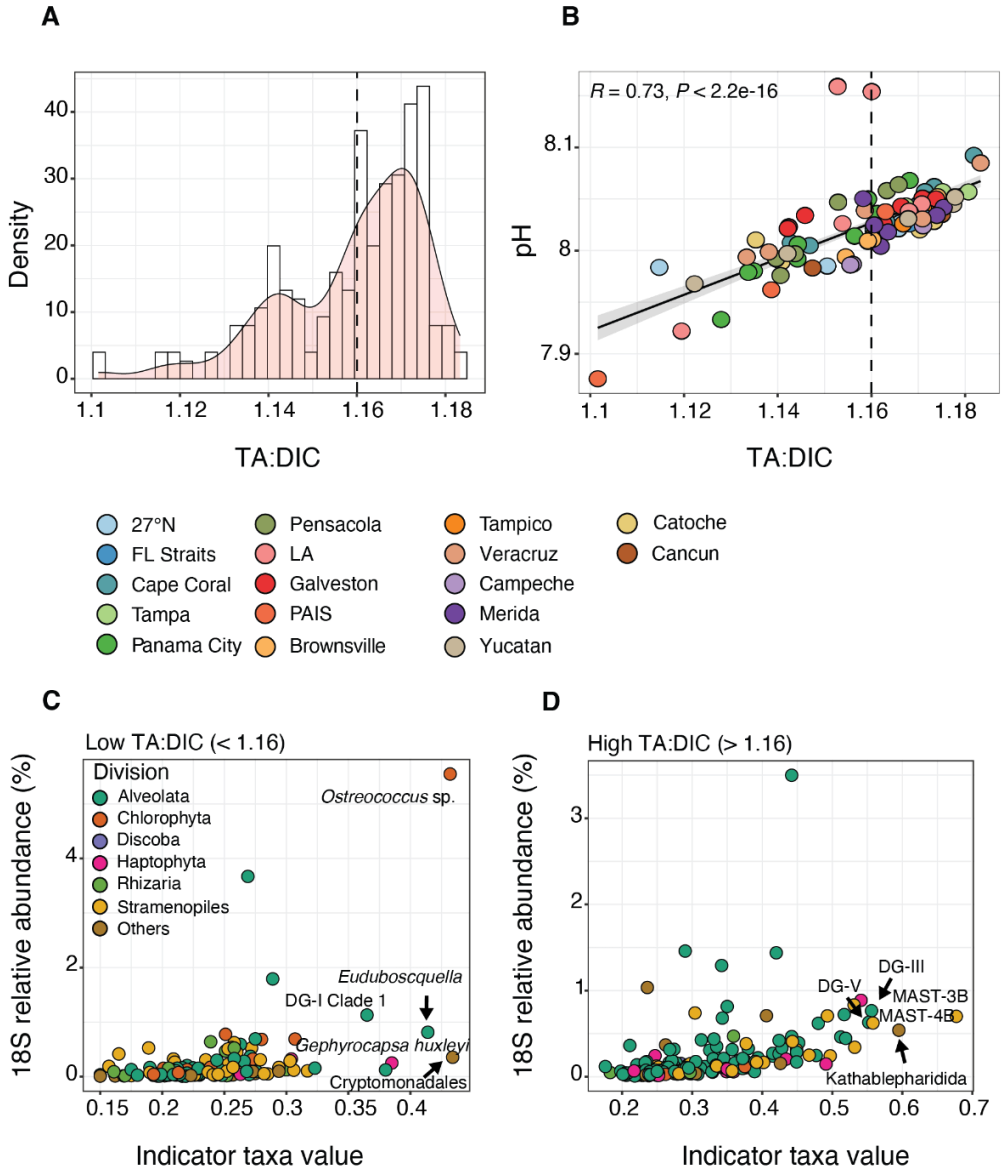

Figure 7: Protist indicator taxa based on TA:DIC ratios in the photic zone. (A) Histogram showing the density distribution of 18S samples in the photic zone (Cluster 1) based on TA:DIC ratios. **(B)** Values of in situ pH vs. TA:DIC in the photic zone, with samples colored by transect. Pearson correlation between variables is shown, with 95% confidence interval. The dotted line in panels **A**–**B** indicate the manual cutoff used for indicator analysis: low TA:DIC < 1.16 vs. high TA:DIC > 1.16. **(C**–**D)** Indicator values vs. average relative abundance (%) for protist ASVs in the photic zone that were significant to the analysis ($P < 0.001$) in samples with either low TA:DIC **(C)** or high TA:DIC **(D)**. Protist ASVs are colored by division and the top five ASVs with the highest indicator values are labeled in each panel, identified to their lowest possible taxonomic assignment (via the PR2 database). DG = Dino-Group. See table S2 for a full list of 18S (and 16S) indicator ASVs. Similar plots for 16S ASVs are shown in fig. S12.

Table 1: Environmental factors used in microbial models. Factors were grouped into parameter type and chosen for initial GLMs based on Spearman correlations (table S1) and low variance inflation factors (VIF < 10) to mitigate collinearity among predictor variables. VIFs varied slightly between 16S and 18S (in parentheses) due to differences in sample size (n = 274 for 16S; n = 235 for 18S) following clustering analysis. Triplicate samples were included in models. Datasets clustered similarly, as evidenced by a similar range in the predictor values. Initial factors were used to construct group-specific models.

Parameter type	Factor	Values	VIF 16S (18S)
Hydrography	Temperature	20.83–30.12 (°C)	2.8 (2.4)
	Salinity	25.16–36.61 (psu)	7 (7.5)
	Oxygen	105.46–232.33 (μmol kg^{-1})	3.1 (5)
Nutrients	Nitrate	0–6.16 (μmol kg^{-1})	4.6 (4.2)
	Phosphate	0–0.85 (μmol kg^{-1})	5.7 (6.2)
	Ammonium	0.12–2.37 (μmol kg^{-1})	1.6 (1.7)
Carbonate chemistry	DIC	1891.67–2186.16 (μmol kg^{-1})	9.1 (8.9)
	pH	7.88–8.16	5.2 (6.1)

Table 2: Final models for major microbial groups in the photic zone. Protists were examined at the class level and prokaryotes at the order level. GLMs were constructed for *Prochlorococcus* and *Synechococcus*. Models were run either with negative binomial (neg bin) or Poisson distributions. Variables that were significant to the final model ($P < 0.05$) are shown for each group and reflect stepwise selection based on Akaike Information Criterion (AIC). See Table 1 for the full list of variables considered. Pseudo R^2 values are shown as a proxy for model fit, though standardized residuals and validation tests confirmed model fit. Temp = temperature (°C); Sal = salinity; Oxy = oxygen (μmol kg^{-1}); PO_4 = phosphate (μmol kg^{-1}); NO_3 = nitrate (μmol kg^{-1}); NH_4 = ammonium (μmol kg^{-1}); DIC = dissolved inorganic carbon (μmol kg^{-1}).

Group	**Taxonomy**	**GLM**	**Type**	R^2
Protists	Dinophyceae	Temp + Sal + Oxy + DIC	Neg Bin	0.5
	Syndiniales	Temp + Sal + PO_4 + NH_4 + pH + DIC	Neg Bin	0.57
	Sagenista	Temp + Oxy + PO_4 + pH	Poisson	0.28
	Prymnesiophyceae	Temp + Sal + PO_4	Poisson	0.6
Prokaryotes	SAR11	Temp + Oxy + NH_4 + DIC	Poisson	0.26
	Synechococcus	Oxy + NO_3 + pH + DIC	Neg Bin	0.38
	Prochlorococcus	Sal + PO_4 + NO_3 + pH	Neg Bin	0.8
	SAR86	Temp + Oxy + NH_4 + pH + DIC	Poisson	0.33
	Flavobacteriales	Sal + DIC	Poisson	0.64